AFRL-RI-RS-TR-2011-029

CROSS-LAYER DESIGN FOR ROBUST AND SCALABLE VIDEO TRANSMISSION IN DYNAMIC WIRELESS ENVIRONMENT

SAN DIEGO STATE UNIVERSITY

FEBRUARY 2011

FINAL TECHNICAL REPORT

APPROVED FOR PUBLIC RELEASE; DISTRIBUTION UNLIMITED.

STINFO COPY

AIR FORCE RESEARCH LABORATORY
INFORMATION DIRECTORATE

■ **AIR FORCE MATERIEL COMMAND** ■ **UNITED STATES AIR FORCE** ■ **ROME, NY 13441**

NOTICE AND SIGNATURE PAGE

AFRL-RI-RS-TR-2011-029 HAS BEEN REVIEWED AND IS APPROVED FOR PUBLICATION IN ACCORDANCE WITH ASSIGNED DISTRIBUTION STATEMENT.

FOR THE DIRECTOR:

/s/

MICHAEL MEDLEY
Work Unit Manager

/s/

WARREN H. DEBANY, Technical Advisor
Information Grid Division
Information Directorate

REPORT DOCUMENTATION PAGE

Form Approved
OMB No. 0704-0188

1. REPORT DATE *(DD-MM-YYYY)*	2. REPORT TYPE	3. DATES COVERED *(From - To)*
February 2011	Final Technical Report	August 2009 – August 2010

4. TITLE AND SUBTITLE

CROSS-LAYER DESIGN FOR ROBUST AND SCALABLE VIDEO TRANSMISSION IN DYNAMIC WIRELESS ENVIRONMENT

5a. CONTRACT NUMBER
FA8750-09-1-0212

5b. GRANT NUMBER
N/A

5c. PROGRAM ELEMENT NUMBER
62702F

6. AUTHOR(S)

Sunil Kurmar
Annamalai Annamalai

5d. PROJECT NUMBER
558B

5e. TASK NUMBER
SD

5f. WORK UNIT NUMBER
PV

7. PERFORMING ORGANIZATION NAME(S) AND ADDRESS(ES)

San Diego State University
Dept of Electrical & Computer Engineering
San Diego CA 92182-1309

Prairie View A&M University
Dept of Electrical & Computer Engineering
Prairie View TX 77446

8. PERFORMING ORGANIZATION REPORT NUMBER

9. SPONSORING/MONITORING AGENCY NAME(S) AND ADDRESS(ES)

Air Force Research Laboratory/RIGF
525 Brooks Road
Rome NY 13441-4505

10. SPONSOR/MONITOR'S ACRONYM(S)
AFRL/RI

11. SPONSORING/MONITORING AGENCY REPORT NUMBER
AFRL-RI-RS-TR-2011-029

12. DISTRIBUTION AVAILABILITY STATEMENT

Approved for Public Release; Distribution Unlimited. This report is the result of contracted fundamental research deemed exempt from public affairs security and policy review in accordance with SAF/AQR memorandum dated 10 Dec 08 and AFRL/CA policy clarification memorandum dated 16 Jan 09.

13. SUPPLEMENTARY NOTES

14. ABSTRACT

Link adaptation is a promising technique for increasing the data rate and spectral efficiency of wireless data-centric networks, without wasting power or sacrificing the bit error rate (BER) performance. The underlying premise of link adaptation is a real-time balancing of the link budget by dynamically adapting the transmitted power level, modulation (signal constellation size), coding rate, block length (symbol rate), or any combination of these parameters to take advantage of prevailing channel conditions. However, conventional adaptive modulation schemes were primarily designed for wireless networks that carry only homogeneous traffic, and thus may not be well suited for next-generation wireless multimedia networks. This report considers the problem of designing an adaptive hierarchical modulation for supporting multimedia transmission over multipath fading channels, in a cross-layer design paradigm. In particular, a method to mechanize a prioritized unicast transmission using hierarchical modulations at the physical layer in response to the disparate quality of service (QoS) requirements for multimedia traffic in an integrated voice/data networks is discussed.

15. SUBJECT TERMS

Wireless Link Adaptation, Cooperative Diversity, Channel Capacity

16. SECURITY CLASSIFICATION OF:			17. LIMITATION OF ABSTRACT	18. NUMBER OF PAGES	19a. NAME OF RESPONSIBLE PERSON
a. REPORT	b. ABSTRACT	c. THIS PAGE			MICHAEL MEDLEY
U	U	U	UU	98	19b. TELEPHONE NUMBER (*Include area code*) N/A

TABLE OF CONTENTS

LIST OF FIGURES

LIST OF TABLES

SUMMARY

Link adaptation is a promising technique for increasing the data rate and spectral efficiency of wireless data-centric networks, without wasting power or sacrificing the bit error rate (BER) performance. The underlying premise of link adaptation is a real-time balancing of the link budget by dynamically adapting the transmitted power level, modulation (signal constellation size), coding rate, block length (symbol rate), or any combination of these parameters to take advantage of prevailing channel conditions. However, conventional adaptive modulation schemes were primarily designed for wireless networks that carry only homogeneous traffic, and thus may not be well suited for next-generation wireless multimedia networks. This report considers the problem of designing an adaptive hierarchical modulation for supporting multimedia transmission over multipath fading channels, in a cross-layer design paradigm. In particular, a method to mechanize a prioritized unicast transmission using hierarchical modulations at the physical layer in response to the disparate quality of service (QoS) requirements for multimedia traffic in an integrated voice/data networks is discussed.

A fundamental technical difficulty in developing a cross-layer design approach for multi-resolution transmission is to find a simple way to effectively match the "shape" of hierarchical modulation at the physical layer to the bit streams with different QoS requirements at the application layer. Unfortunately, for most non-binary modulation techniques, exact closed-form expressions for the BER are hard to find and they are also not easily invertible with respect to their arguments. But these properties are needed for adaptive modulation design. Hence, this report first develops BER approximations for both hierarchical quadrature amplitude modulation (QAM) and hierarchical phase shift keying (PSK) modulation schemes in terms of exponential and complementary error functions by curve fitting. The efficacy of the complimentary error function approximation as a better curve fitting

approximation in comparison to exponential approximation is established. Secondly the importance of a readily invertible equation for a matched hierarchical modulation design is demonstrated.

Two additional applications of the invertible BER approximations are also discussed. In the first application, the efficacy of a receiver-oriented rate-adaptation scheme is investigated using hierarchical QAM for sustaining the quality of randomly fluctuating wireless links in mobile ad-hoc networks at a desired level. This is done by multiplexing and mapping different traffic sources that require unequal error protection into a hierarchical modulation. In the second application, the efficacy of adaptive multi-resolution modulation for multimedia transmission over flat fading channels is studied. In this case, an adaptive hierarchical modulation signaling technique is designed to take advantage of the differences in the QoS requirements among different bit streams at the application layer. Finally, the joint design of convolutional codes and asymmetric modulation is discussed for unequal error protection of H.264/AVC compressed video bitstreams for increased robustness when transmitting over fading channels.

1.0 INTRODUCTION

1.1 Motivation

Contemporary wireless systems are faced with many challenges for supporting multimedia traffic. Such challenges include limited battery life and fluctuation of the wireless link. Link adaptation is a promising technique for increasing the data rate and spectral efficiency of wireless data-centric networks. This is done without wasting power or sacrificing the bit error rate (BER) performance. The fundamental principle of link adaptation is a real-time balancing of the link budget. Modulation parameters such as transmitted power level, signal constellation size, coding rate, block length (symbol rate), or any combination of these parameters are dynamically adapted to take advantage of prevailing channel conditions. As compared to other adaptive schemes, the adaptive signaling techniques presented here carries heterogeneous traffic and are suited for next-generation wireless multimedia networks that need to support a wide range of data rates and reliability requirements.

Adaptive modulation design requires invertible BER approximations because the exact bit error rate expressions are not easily inverted. Chung et al. [1] presented a systematic study on transmitter oriented adaptive modulation and demonstrated the impact on spectral efficiency of adapting for various modulation parameters under different symmetric constellation restriction and BER constraints. In so doing the authors developed an approximation for the exact BER in order to obtain the optimal power and rate adaptation for different modulation scheme by curve fitting.

It has been shown in [2, 3, 27] that to improve the efficiency in a time varying network such as mobile ad-hoc (MANET), for a constant signaling rate (i.e. fixed signal constellation size), the shape of the asymmetry PSK can be designed to match the unequal error protection (UEP) requirement for different classes of traffic. However adapting the "shape" of the constellation alone may not be adequate

to maximize the spectral utilization efficiency. Thus, joint design of the transmitter-oriented rate adaptation and the receiver-oriented rate adaptation might be more appropriate to take advantage of the differences in the quality of service (QoS) disparity among different traffic sources.

Seminal work found in by Hayes [4], Cavers [5], Hentinen [6] and Annamalai et al [7, 8] on link adaptation illustrated that in a time-varying wireless network, the spectral utilization network efficiency can be improved dynamically by link adaptation technique. However, the classical transmitter-oriented rate adaptation method suffers from a number of shortcomings, such as:

(1) It generally requires instantaneous feedback of the channel state or channel side information (CSI) from the receiver to the sender.

(2) It is normally accompanied with an increase in the complexity of the transmitter design.

(3) Its practicality is limited to slowly time-varying channel.

Taking into account the fixed signal constellation size and shortcomings, this project has considered the problem of designing adaptive hierarchical modulation for supporting multimedia traffic over generalized multipath fading channels. Many papers have been published on adaptive modulation, however, all previous work done on adaptive modulation with the exception of M. Pursley [9] and Hossain [10] were designed for networks that carry only homogeneous traffic. In this project the signal design is more general than the asymmetric PSK considered by Pursley [9] and takes into account the effects of channel fading.

The seminal work done by T. Cover [11] on the capacity of broadcast channels has established that the optimal broadcast and multicast scenarios are multi-resolution or embedded in character due to the competitive nature of broadcast signaling. That is the maximum information rate to one user is constrained by the rate of information sent to the other users. In fact, the result from Cover [11] shows that superimposing the “coarse” information within the “fine” information is generic in scope, and

places no restrictions on the domain in which embedding should be executed. Inspired by this information-theoretic work, several digital modulation techniques that employ asymmetric signal constellation have received substantial attention. Some of these works in digital modulation techniques are in digital video broadcasting and was done by Ramchandran [12] and Chan [13]. Digital modulation techniques works were also done in multicasting multimedia messages to receivers of different capabilities by Sajadieh [14] and Pursley [16].

In this report, BER approximation for both hierarchical quadrature amplitude modulation (QAM) and hierarchical phase shift keying (PSK) modulation schemes are first developed in terms of exponential and complementary error functions by curve fitting. The usefulness of the complimentary error function approximation as a better curve fitting approximation in comparison to exponential approximation is shown. Then the importance of a readily invertible equation for a matched hierarchical modulation design is demonstrated. The resulting embedded gain can be translated into energy and/or spectral efficiency improvement over the traditional uniform (symmetric) modulation design.

The invertible BER approximations are employed in two applications. The first application investigates the efficacy of a receiver-oriented rate-adaptation scheme using hierarchical QAM for maintaining the quality of randomly fluctuating wireless links in mobile ad-hoc networks at a desired level. This is achieved by multiplexing and mapping different traffic sources that require unequal error protection into a hierarchical modulation and dropping the “less important” bits when the channel conditions worsen. This passive rate-adaptation method is motivated by the need to allow for graceful signaling rate reduction in wireless ad-hoc networks when the channel condition deteriorates for a short period of time, rather than declaring a link outage (which necessitates the search for a new route path and incur considerable delay and overhead) and avoid costly frequent re-routing.

In the second application, the efficacy of adaptive multi-resolution modulation for multimedia transmission over flat fading channels is studied. In this scheme, adaptive hierarchical modulation signaling technique is studied. The design takes advantage of the differences in the QoS requirements among different bit streams at the application layer. The size of digital signal constellation is adapted based on the prevailing channel conditions. This is done with the goal of improving the spectrum utilization efficiency without wasting power or forfeiting BER performance. *Finally,* the joint design of convolutional codes and asymmetric modulation is discussed for unequal error protection of H.264/AVC compressed video bitstreams for increased robustness when transmitting over fading channels. In this application, the inherent UEP capability of the H.264/AVC video bitstreams at the application layer is combined with equal code rate convolutional codes or prioritized Rate-Compatible Punctured Convolutional (RCPC) codes and hierarchical 8PSK modulation at the physical layer. The entire ensemble is referred to as a multi-layer UEP system and designs as well as implementations of overall code rates 1/2, 2/3, 3/4 and 4/5 are considered.

1.2. Objectives

This report considers the problem of designing an adaptive hierarchical modulation for supporting multimedia transmission over multipath fading channels in a cross-layer design paradigm. The adaptive hierarchical modulation consists of non-uniformly spaced signal constellation points that permit unequal error protection of transmitted bits within a symbol according to their importance. The objectives of this report are:

i. To develop BER approximations for hierarchical quadrature amplitude modulation (QAM) scheme in terms of complementary error function.

ii. To demonstrate the efficacy of the complimentary error function approximation as a better curve fitting approximation in comparison to exponential approximation.

iii. To show the importance of a readily invertible equation for a matching hierarchical modulation design.

iv. To investigate the efficacy of a receiver-oriented rate-adaptation scheme using hierarchical QAM.

v. To study the efficacy of adaptive multi-resolution modulation for multimedia (including H.264 video) transmission over flat fading channels.

1.3 Organization of Report

Chapter 1 provides the motivation for this effort and the literature review. Chapter 2 introduces both the BER exponential and BER complementary error function approximations. The two BER approximations are compared to the exact BER by curve fitting for both average bit error rate and individual bit error rate. For a matching hierarchical modulation design the BER complementary error function approximation is inverted.

In Chapter 3, the receiver-oriented rate-adaptation scheme is investigated using hierarchical QAM. The importance of the scheme and invertible BER equation are demonstrated; and the optimum beta value algorithm is also shown with an example. The steady state probability of discrete Markov chains is employed to obtain the decision area of the receiver. At the end of this chapter, various plots of the spectral efficiency are shown for different values of beta. The efficacy of adaptive multi-resolution modulation for multimedia transmission over flat fading channels is studied in Chapter 4. Based on the channel condition, the scheme decides the best modulation scheme to employ in order to meet the required QoS. In concluding Chapter 4, plots of the spectral efficiency and the performance of the scheme in different Nakagami channels are shown. In Chapter 5, the joint design of convolutional codes and asymmetric modulation is discussed for unequal error protection of H.264/AVC compressed video bitstreams for increased robustness when transmitting over fading channels. In this application, the

inherent UEP capability of the H.264/AVC video bitstreams at the application layer is combined with equal code rate convolutional codes or prioritized RCPC codes and hierarchical 8PSK modulation at the physical layer. In Chapter 6, the conclusions, report contributions, future research and recommendation are presented.

2.0 BACKGROUND AND ASSUMPTIONS

2.1 System Model for Hierarchical M-QAM

In a situation where unequal error protection is needed for various bits in a symbol; the construction of a specific PSK and QAM constellation is required. To obtain unequal error protection, multicast PSK and QAM constellations are made up of non-uniformly spaced symbols to allow different degrees of protection for transmitted bits within a symbol with respect to their importance. Vitthaladevuni and Alouini [18,19] have derived a generic expression for the exact bit error rate (BER) computation of generalized hierarchical M-ary QAM and M-ary PSK over additive white Gaussian noise channel. These generic expression for the exact bit error rate in are bit one and bit two of the 4-PAM and bit one, bit two and bit three of the 8-PAM [18, 19].

2.1.1 Hierarchical QAM

Figure 1 shows a generalized hierarchical M-ary QAM signal constellation with grey code mapping where $2d_1$, $2d_2$ and $2d_3$ indicates the distances between points in the first, second and third level of hierarchy, respectively. The relationship between the distances is given by:

$$\frac{d_{i+1}}{d_i} = \beta, i = 1,2,..., m-1 \quad (1)$$

where β is the constellation shape parameter. The three highest priority bits are given the MSB position in the in-phase (I) and the quadrature phase (Q) respectively. Bits with lower priorities are given the subsequent position of the lower significance.

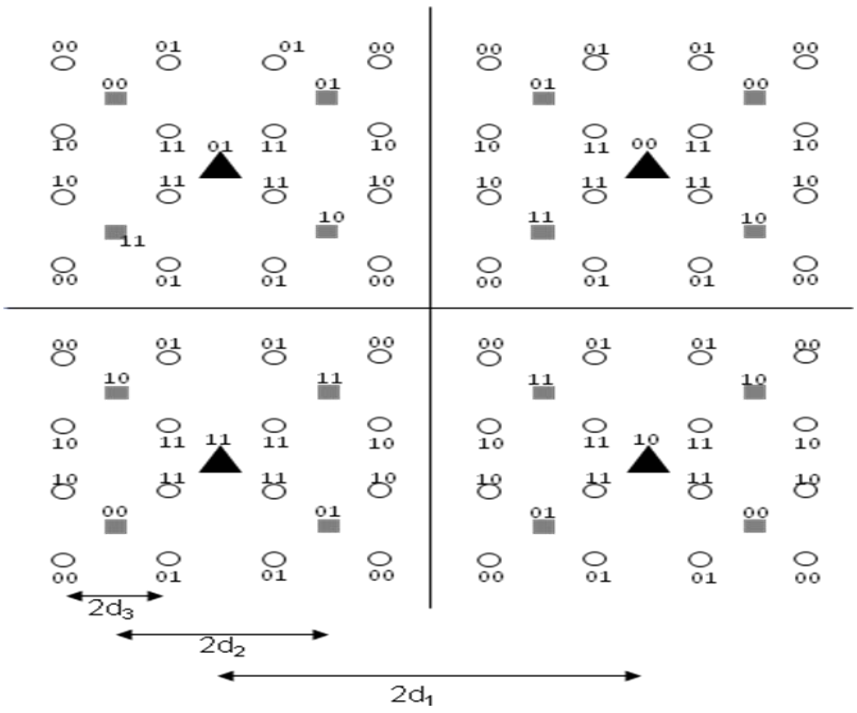

Figure 1: Generalized Hierarchical Square 4/16/64-QAM Signal constellation

2.1.2 Transformation of 16 and 64 QAM from Generalized 4 and 8 PAM

Using the generalized 4 and 8 PAM equations [18], the exact BER for 16-QAM and 64-QAM equations can be obtained as a function of β and γ. The following shows the procedure for transforming the first bit of the 4-PAM equation into the first bit expression of 16-QAM using the definitions found in Vitthaladevuni and Alouini [19]. From [18],

$$P_b^{QAM}(M_\gamma^\beta, i) = P_b^{PAM}(\sqrt{M_\gamma^\beta}, i) \tag{2}$$

$$d_k = d_m \beta^{k-m} \tag{3}$$

where $\mathrm{m} = \frac{1}{2}\log_2 M$ and k = 1, 2..., m and

$$\frac{Cd_m}{\sqrt{N_0}} = \pm\sqrt{G(C,p)\gamma} = \mathrm{sgn}(C)\sqrt{|C|\gamma} \tag{4}$$

where $G(C, p) = \frac{C^2}{pp^T}$.

The 4-PAM equation for bit one is given by

$$P_b(4, d, i_1) = \frac{1}{2}\left[\frac{1}{2} erfc \frac{d_1 + d_2}{\sqrt{N_0}} + \frac{1}{2} erfc \frac{d_1 - d_2}{\sqrt{N_0}}\right] \quad (5)$$

where d is the distance vector d= $d_1, d_2 ..., d_m$

For 16 QAM M=16

From Equations (2) and (3)

$$m = \frac{1}{2}\log_2 16 = 2 \qquad \text{k= 1, 2}$$

since $d_k = d_m \beta^{k-m}$.

For m= 2 and k=1:

$$d_1 = d_2 \beta^{-1} \Rightarrow \beta^{-1} = \frac{d_1}{d_2}$$

For m=2 and k=2:

$$d_2 = d_2 \beta^0 \Rightarrow \beta^0 = \frac{d_2}{d_2}$$

Substituting $d_1 = d_2 \beta^{-1}$ into (5) yields

$$P_b(4, d, i_1) = \frac{1}{2}\left[\frac{1}{2} erfc \frac{d_2(\beta^{-1} + 1)}{\sqrt{N_0}} + \frac{1}{2} erfc \frac{d_2(\beta^{-1} - 1)}{\sqrt{N_0}}\right] \quad (6)$$

since

$$\frac{d_m}{\sqrt{N_O}} = \sqrt{\frac{\gamma}{2pp^T}}$$

where p is priority vector as

$$p = [p_1, p_{2,...,} p_{m-1}, p_m] = \left[\frac{d_1}{d_m}, \frac{d_2}{d_m}, ..., \frac{d_{m-1}}{d_m}, 1\right]. \quad (7)$$

For m=2, Equation (7) becomes

$$p = \left[\frac{d_1}{d_2}, \frac{d_2}{d_2} \right] = \left[\beta^{-1}, \beta^{0} \right]$$

Therefore, transposing p

$$pp^T = \left[\ \beta^{-1} \beta^{0} \ \right] \begin{bmatrix} \beta^{-1} \\ \beta^{0} \end{bmatrix} = \left[\beta^{-2} + 1 \right]$$

results in

$$\frac{d_m}{\sqrt{N_O}} = \sqrt{\frac{\gamma}{2(\beta^{-2}+1)}} \ .$$

Substituting this expression into Equation (6) the first bit for 16-QAM gives

$$P_b^{QAM}(16_\gamma^\beta, \beta, i_1) = \frac{1}{2}\left[\frac{1}{2} erfc\left((\beta^{-1}+1)t\right) + \frac{1}{2} erfc\left((\beta^{-1}-1)t\right) \right] \tag{8}$$

Following the same steps above the second bit for 4/16 QAM yields

$$P_b^{QAM}(16_\gamma^\beta, \beta, i_2) = \frac{1}{4}\left[2erfc(t) - erfc\left((2\beta^{-1}+1)i\right) + erfc\left((2\beta^{-1}-1)t\right) \right] \tag{9}$$

where $t = \sqrt{\frac{\gamma}{2(\beta^{-2}+1)}}$

Equations (8) and (9) above are the first and second bit class for 16 QAM, respectively, written in terms of β and γ. Following the exact procedure detailed above for 16-QAM, the exact equations for the 64-QAM are derived from 8-PAM with the first bit for 64-QAM given by

$$\begin{aligned} P_b^{QAM}(64_\gamma^\beta, \beta, i_1) = \frac{1}{8}[& erfc\left((t)(\beta^{-2} - \beta^{-1} + 1)\right) + erfc\left((t)(\beta^{-2} - \beta^{-1} - 1)\right) \\ & + erfc\left((t)(\beta^{-2} + \beta^{-1} - 1)\right) + \left((t)(\beta^{-2} + \beta^{-1} + 1)\right)] \end{aligned} \tag{10}$$

and the second bit for 64-QAM expressed as

$$P_b^{QAM}(64_\gamma^\beta,\beta,i_2)=\frac{1}{8}[2erfc\big((t)(\beta^{-1}-1)\big)-erfc\big((t)(2\beta^{-2}+\beta^{-1}+1)\big)$$

$$+erfc\big((t)(2\beta^{-2}-\beta^{-1}-1)\big)+2erfc\big((t)(\beta^{-1}+1)\big)-erfc\big((t)(2\beta^{-2}-\beta^{-1}+1)\big) \quad (11)$$

$$+erfc\big((t)(2\beta^{-2}+\beta^{-1}-1)\big)]$$

The third bit for 64-QAM is

$$P_b^{QAM}(64_\gamma^\beta,\beta,i_3)=\frac{1}{8}[4erfc(t)+2erfc\big((2t)(\beta^{-1}-1)\big)+erfc\big((t)(2\beta^{-2}-2\beta^{-1}+1)\big)$$

$$+2erfc\big((2t)(\beta^{-1}+1)\big)-erfc\big((t)(2\beta^{-2}-2\beta^{-1}-1)\big)+2erfc\big((2t)(\beta^{-2}-1)\big) \quad (12)$$

$$+2erfc\big((2t)(\beta^{-2}+1)\big)+erfc\big((2t)(\beta^{-2}+2\beta^{-1}-1)\big)-erfc\big((2t)(\beta^{-2}+2\beta^{-1}+1)\big)]$$

where t= $\sqrt{\frac{\gamma}{2(\beta^{-4}+\beta^{-2}+1)}}$

2.2 Bit Error Probability

2.2.1 Approximated BER for QAM

Annamalai et al [17] has been shown that matching the distinct requirement for multimedia source to the shape of the multicast modulation leads to significant modulation embedding gain. Nevertheless to find the optimal shape of the multicast constellation, the exact bit error rate equation for 16-QAM and 64-QAM developed in Section 2.1.2 are not readily invertible with respect to its symbol SNR (γ). Since the exact equations are not readily invertible, approximation for the BER were developed using the exponential function [17]. The same procedure outlined by Annamalai et al [17]

is followed to obtain an approximation for the BER using complementary error function expressions for 16-QAM and 64-QAM. The complementary error function is given by

$$erfc(x) = \frac{2}{\sqrt{\pi}} \int_{x}^{\infty} e^{-t^2} dt = 1 - erf(x) \tag{13}$$

erf(x) is the error function and is defined by twice the integral of the Gaussian distribution with 0 mean and variance of 0.5. The error function is given by

$$erf(x) = \frac{2}{\sqrt{\pi}} \int_{0}^{x} e^{-t^2} dt \tag{14}$$

From [17], the Exponential approximation is

$$P_b^{(i)}(\gamma_s, \beta) = a_\beta^{(i)} e^{-b_\beta^{(i)} \cdot \gamma_s} + c_\beta^{(i)} e^{-2b_\beta^{(i)} \cdot \gamma_s} \tag{15}$$

Similarly the complementary error function approximation is

$$P_b^{(i)}(\gamma_s, \beta) = a_\beta^{(i)} erfc\left(\sqrt{\gamma_s b_\beta^{(i)}}\right) + c_\beta^{(i)} erfc^2\left(\sqrt{\gamma_s b_\beta^{(i)}}\right) \tag{16}$$

where i = 1, 2, 3..., $\log_2 M$ and β is the phase offset ratio for PSK or is the constellation shape parameter for QAM; $a_\beta^{(i)}, b_\beta^{(i)}$ and $c_\beta^{(i)}$ are three parameters to be determined such that the difference between the exact BER and the approximation is minimized in the sense of mean square error. The Quasi-Newton BFGS algorithm is used to perform the curve fitting. Further simplification can be done to $a_\beta^{(i)}$, $b_\beta^{(i)}$ and $c_\beta^{(i)}$ by using the following 3rd order polynomial expression: $p_3\beta^3 + p_2\beta^2 + p_1\beta + p_o$

Where P_3, P_2, P_1 and P_0 are constant to be determined.

The following section summaries the polynomial coefficients and the plots of the curve fitting for 4-PSK, 8-PSK, 16-QAM and 64-QAM. The results in Section 2.2.2 extend on the work done by Annamalai et al [1]. The BER complementary error function

approximation i.e. Equation (16) is utilized to curve fit for both PSK and QAM. Equations (15) and (16) were derived with the help of the Quasi-Newton unconstrained optimization algorithm.

2.2.2 Probability of Bit Error 16-QAM and 64-QAM

In Section 2.1.2 the transformation from generalized 4 and 8 PAM to 16 and 64-QAM was done and also in Section 2.2.1 the BER approximation expression using erfc was developed, i.e. Equation (16). Having completed these two tasks, curve fitting for 16-QAM and 64-QAM is done by using the previously developed exponential approximation (Equation (15)) is now done by the BER complementary error function approximation. Using the new approximation developed in Section 2.2.1 (Equation (16)) curve fitting for the individual and average bit error rate (BER) for 4-PSK, 8-PSK, 16-QAM and 64-QAM are carried out. The curve fitting exercise verifies the exactness of the complementary error function approximation. Finally the comparison between erfc and exponential BER approximation is done in order to demonstrate that erfc approximation produces better curve fitting results. The polynomial coefficients alone with their respective curve fit are summarized in this section.

Curve fitting results for 16-QAM using both approximation expressions are shown below in Figures 2 and 3. The polynomial coefficients $a_{\beta}^{(i)}, b_{\beta}^{(i)}$ and $c_{\beta}^{(i)}$ for the exponential function and complementary error function approximation are listed below in Tables 1 and 2, respectively. A close inspection of these the initial results (Figures 2 and 3) reveals that the complementary error function gives better curve fitting result than the exponential function. That is using the complementary error function approximation; the curve fitting result is close to the exact bit error rate curve.

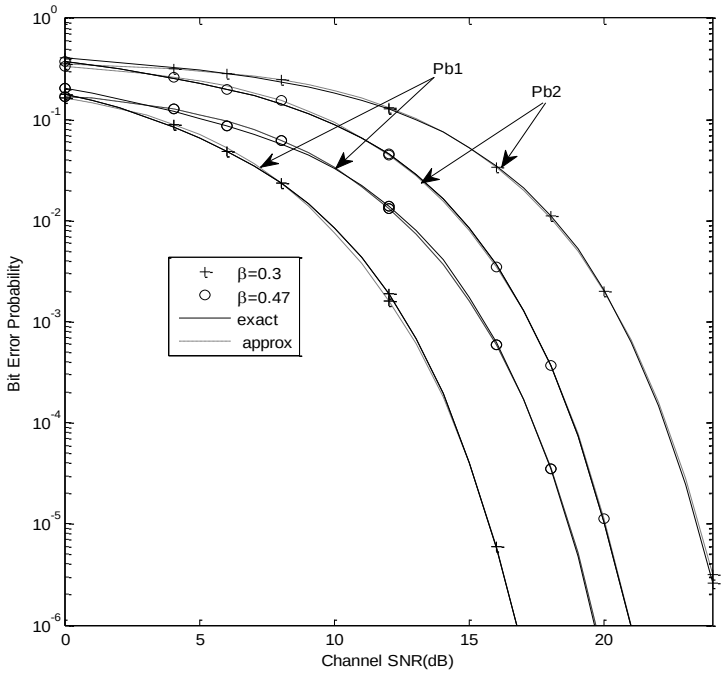

Figure 2: Exact and Approximate BER Curves for 16-QAM Using Exponential Function Approximation

Table 1. Polynomial Coefficients for 16-QAM Using Exponential Function Approximation

i		p_3	p_2	p_1	p_0
1	$a_\beta^{(1)}$	-1.207	1.160	-0.294	0.074
	$b_\beta^{(1)}$	0.358	0.319	-1.060	0.509
	$c_\beta^{(1)}$	-0.231	1.448	-1.256	0.436
2	$a_\beta^{(2)}$	-3.243	3.972	-1.493	0.309
	$b_\beta^{(2)}$	-0.372	0.666	-0.034	0.002
	$c_\beta^{(2)}$	0.968	-1.208	0.453	0.191

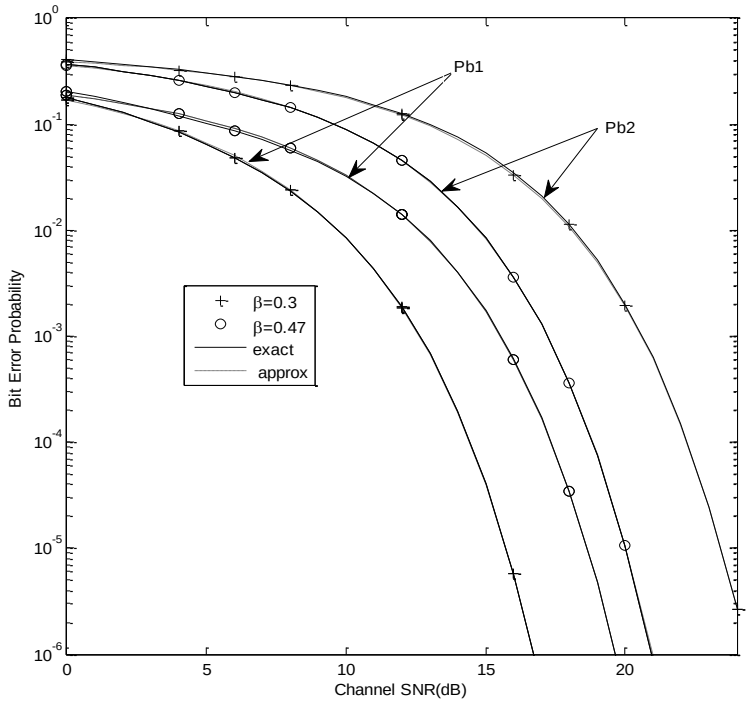

Figure 3: Exact and Approximate BER Curves for 16-QAM Using Complementary Error Function Approximation

Table 2. Polynomial Coefficient for 16-QAM Using Complementary Error Functions Approximation

i		p_3	p_2	p_1	p_0
1	$a_\beta^{(1)}$	-1.209	1.369	-0.518	0.309
	$b_\beta^{(1)}$	0.308	0.376	-1.076	0.505
	$c_\beta^{(1)}$	-5.352	8.105	-4.444	0.937
2	$a_\beta^{(2)}$	-23.829	20.682	-5.027	0.757
	$b_\beta^{(2)}$	-0.170	0.185	0.228	-0.038
	$c_\beta^{(2)}$	25.976	-22.158	5.396	-0.276

Next curve fitting is done for the average BER probability for 16-QAM. This is because the proposed adaptive multi-resolution scheme uses the average BER probability to

determine which modulation scheme to use for specified BER requirement. Again curve fitting for the average BER probability using both approximation expressions and compare the result. Since there are two bit classes in 16-QAM average BER probability ($\bar{P}_b$) for 16-QAM is given by

$$\bar{P}_b = \frac{P_b^{(1)} + P_b^{(2)}}{2} \tag{17}$$

Tables 3 and 4 depict the polynomial coefficients for the average bit error probability for 16-QAM signal constellation using the erfc and exponential function equations approximation, respectively. Figure 4 and 5 compares the two plots of the exponential and complementary error function, respectively. This comparison further reveals that the curve fitting using the complementary error function approximation gives better result than exponential function approximation.

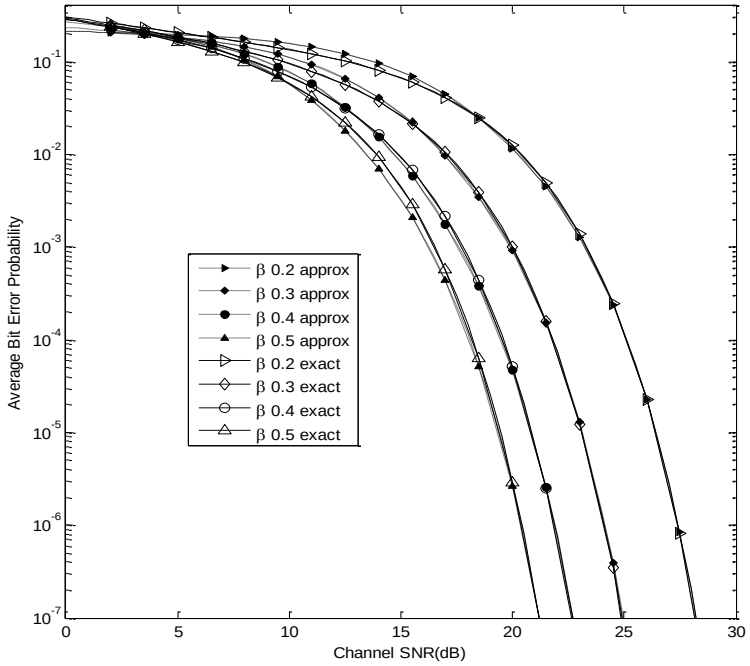

Figure 4: Exact Average BER and Approximate Average BER Curves for 16-QAM Using Exponential Function Approximation

Table 3. Average BER Polynomial Coefficients for 16-QAM Using Exponential Function Approximation

	p_3	p_2	p_1	p_0
a_β	4.561	-3.894	0.975	-0.005
b_β	-0.280	0.530	0.012	-0.001
c_β	4.265	-2.793	0.777	0.072

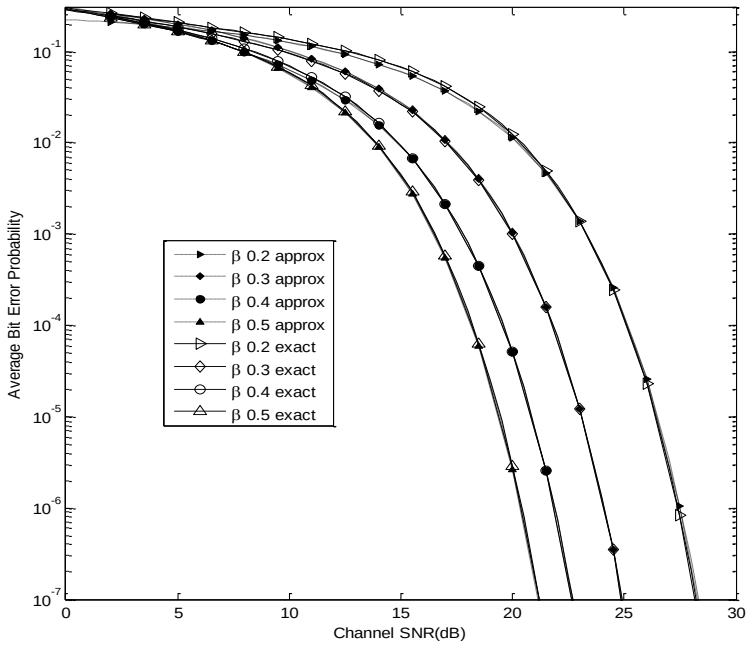

Figure 5: Exact Average BER and Approximate Average BER Curves for 16-QAM Using Complementary Error Function Approximation

Table 4. Average BER Polynomial Coefficients for 16-QAM Using Complementary Error Function Approximation

	p_3	p_2	p_1	p_0
a_β	29.947	-29.791	9.691	-0.775
b_β	-0.096	0.317	0.089	-0.011
c_β	-30.417	27.253	-6.667	0.561

2.2.3 Probability of Bit Error 64-QAM

In this section similar results as in Section 2.2.2 is expected and so curve fitting for 64-QAM by using the BER approximation expressions (i.e. Equation (15) and (16)) is obtained. The results of the curve fitting for the individual bit for 64-QAM using exponential function is shown below in Figure 6 and 7. The coefficients for these figures

are given in Tables 5 and 6. As mentioned in Section 2.2.2 of the average BER probability is needed to determine which modulation scheme to use for specified BER requirement. Tables 7 and 8 show the coefficients for average BER for 64-QAM using complementary error function and exponential function. Figures 8 and 9 show the average plot BER plot for 64-QAM. For 64-QAM, there is three bit classes. Therefore, the average BER probability ($\bar{P}_b$) for 64-QAM is given by

$$\bar{P}_b = \frac{P_b^{(1)} + P_b^{(2)} + P_b^{(3)}}{3} \tag{18}$$

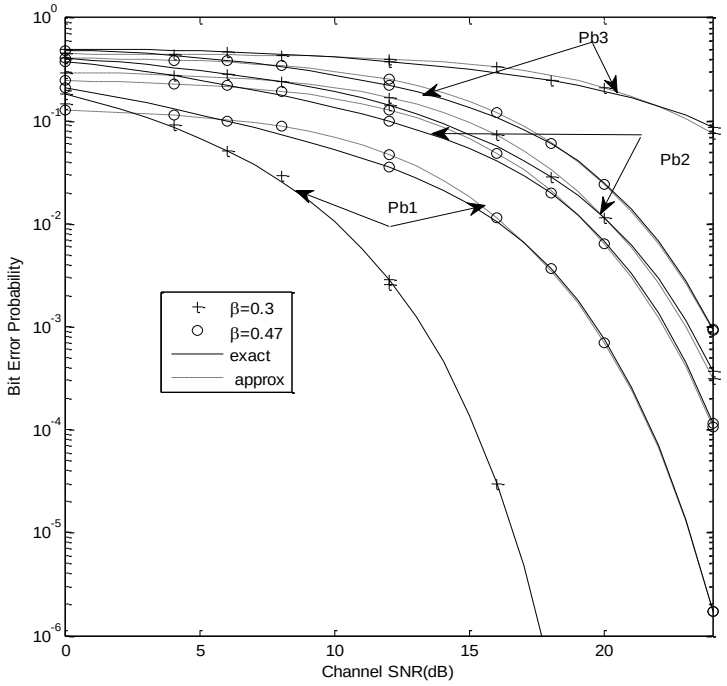

Figure 6: Exact BER and Approximate BER Curves for 64-QAM using Exponential Function

Table 5. Polynomials for 64-QAM Using Exponential Function Approximation

i		p_3	p_2	p_1	p_0
1	$a_\beta^{(1)}$	-1.253	1.361	-0.459	0.079
	$b_\beta^{(1)}$	2.143	-0.958	-1.025	0.510
	$c_\beta^{(1)}$	2.755	-1.237	-0.711	0.423
2	$a_\beta^{(2)}$	0.851	0.765	-1.021	0.295
	$b_\beta^{(2)}$	-0.311	0.123	0.068	-0.001
	$c_\beta^{(2)}$	-0.413	-0.440	0.264	0.199
3	$a_\beta^{(3)}$	2.953	-3.546	0.832	0.228
	$b_\beta^{(3)}$	0.272	-0.064	0.014	0.000
	$c_\beta^{(3)}$	-0.511	1.589	-0.608	0.267

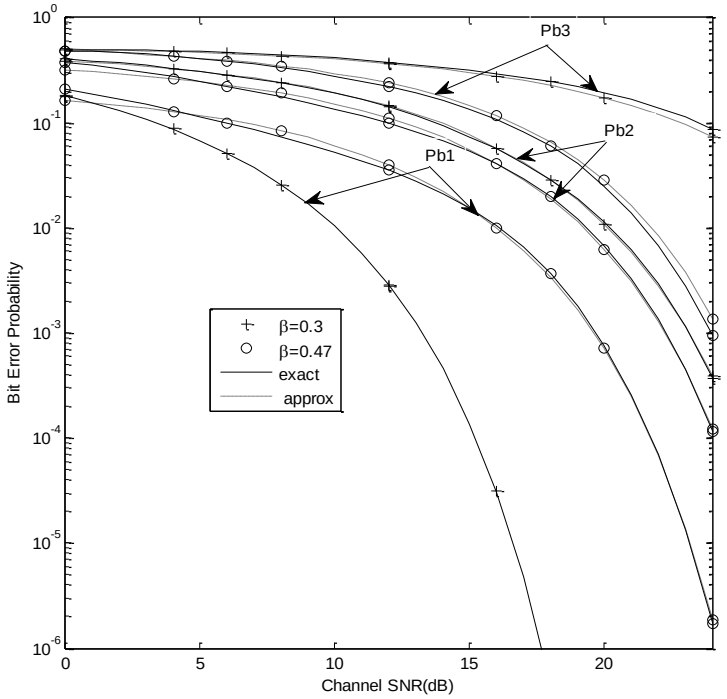

Figure 7: Exact BER and Approximate BER Curves for 64-QAM Using Complementary Error Function Approximation

Table 6. Polynomial for 64-QAM BER Using Complementary Error Function Approximation

i		p_3	p_2	p_1	p_0
1	$a_\beta^{(1)}$	-3.414	3.826	-1.573	0.350
	$b_\beta^{(1)}$	1.540	-0.349	-1.211	0.523
	$c_\beta^{(1)}$	0.751	2.763	-3.609	1.144
2	$a_\beta^{(2)}$	38.907	-43.232	15.503	-1.588
	$b_\beta^{(2)}$	2.563	-3.093	1.237	-0.141
	$c_\beta^{(2)}$	-31.354	34.723	-12.872	1.867
3	$a_\beta^{(3)}$	98.777	-98.649	30.834	-2.639
	$b_\beta^{(3)}$	6.527	-5.921	1.704	-0.157
	$c_\beta^{(3)}$	-99.468	99.431	-30.864	3.144

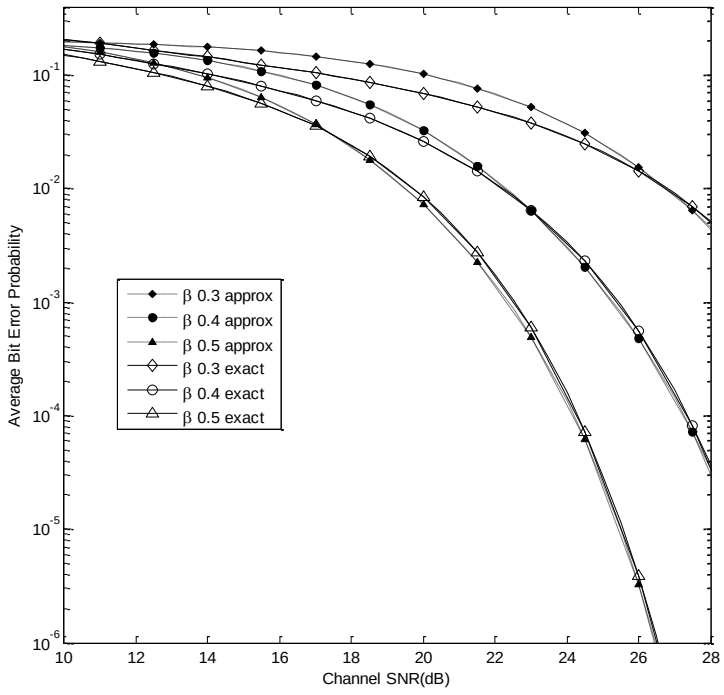

Figure 8: Exact Average BER and Approximated Average BER Curves for 64-QAM Using Exponential Function Approximation

Table 7. Average BER Polynomial Coefficients for 64-QAM using Exponential Function Approximation

	p_3	p_2	p_1	p_0
a_β	10.57	-9.499	2.441	-0.091
b_β	0.204	0.021	-0.012	0.000
c_β	-10.555	8.301	-1.146	-0.003

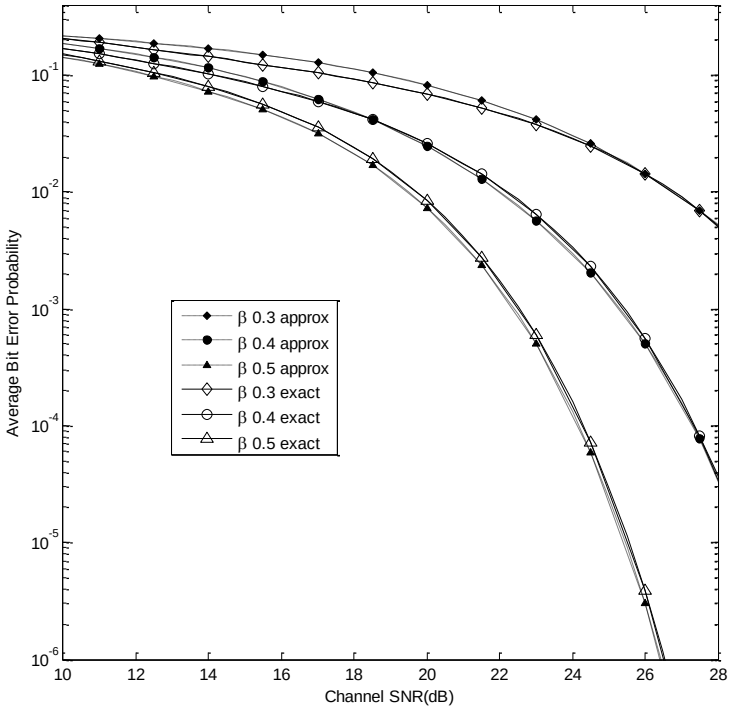

Figure 9: Exact Average BER and Approximated Average BER Curves for 64-QAM Using Complementary Error Function Approximation

Table 8. Average BER Polynomial Coefficients for 64-QAM Using Complementary Error Function Approximation

	p_3	p_2	p_1	p_0
a_β	14.474	-11.337	2.735	-0.061
b_β	0.179	0.055	-0.028	0.001
c_β	31.334	-30.128	0.942	-0.674

2.2.4 Hierarchical 4 and 8 PSK

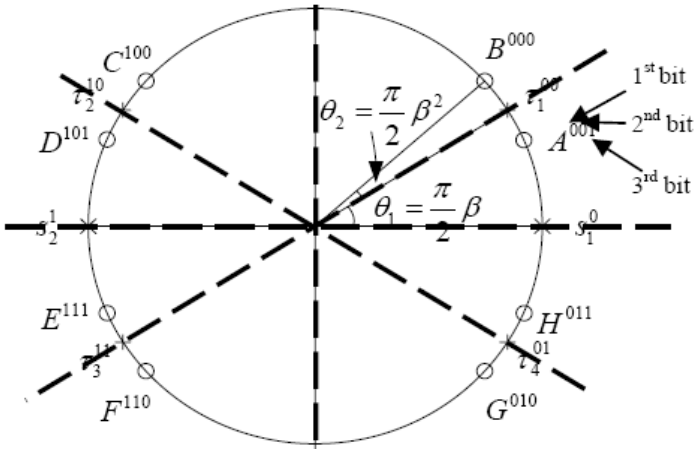

Figure 10: Asymmetric 8-PSK constellations

Previous work done by Annamalai et al [2], the asymmetric 8-PSK shown in Figure 10 was proposed and the approximation expression for the BER probability was obtained with Equation (15). The authors [2] consider a generalized 2/4/…/M-PSK constellation with Karnaugh map style Gray mapping as seen in Figure 10 for the generalized 8-PSK. This procedure of Gray coding ensures the greatest protection to the most significant bit (MSB) at the cost of the least significant bit (LSB). The angles used in the work evolve in a hierarchy. Since the receiver oriented adaptive rate system is

operating at a constant power and signaling rate, the receiver adapts its modulation scheme base on the existing channel condition. In the above 4-PSK constellation is embedded in the 8-PSK constellation and is marked by the '+'. It is worth noting that for the same transmission power, a smaller size constellation creates a larger Euclidean distance between the signal points. Hence, better immunity against channel fading and noise. θ_i is the phase offset angle and is given by

$$\theta_i = \frac{\pi}{2}\beta^i, i = 1,2,..m-1 \quad (19)$$

where m= $\log_2 M$ and M is the alphabet size

The work done by Annamalai et al [1] is extended by showing that erfc approximation curve fitting is better than the exponential function. Finally the erfc BER approximation is compared to exponential BER approximation for both individual and average bit.

2.2.5 Probability of Bit Error 4-PSK

The curve fitting results for the approximate BER probability and the exact BER probability for 4-PSK is shown in Figures 11 and 12 along with their respective polynomial coefficients in Tables 9 and 10. To generate the exact curve for 4-PSK the exact Equations (20) and (21) shown below are utilized.

The exact equations for 4-PSK are

$$P_b^{(1)}(\gamma_s, \alpha) = \frac{1}{2} erfc(\sqrt{\gamma_s} \cos\frac{\pi}{2}\alpha) \quad (20)$$

$$P_b^{(2)}(\gamma_s, \alpha) = \frac{1}{2} erfc(\sqrt{\gamma_s} \sin\frac{\pi}{2}\alpha) \quad (21)$$

where $\gamma_{(s)}$ is the CNR in dB and α is the phase offset ratio

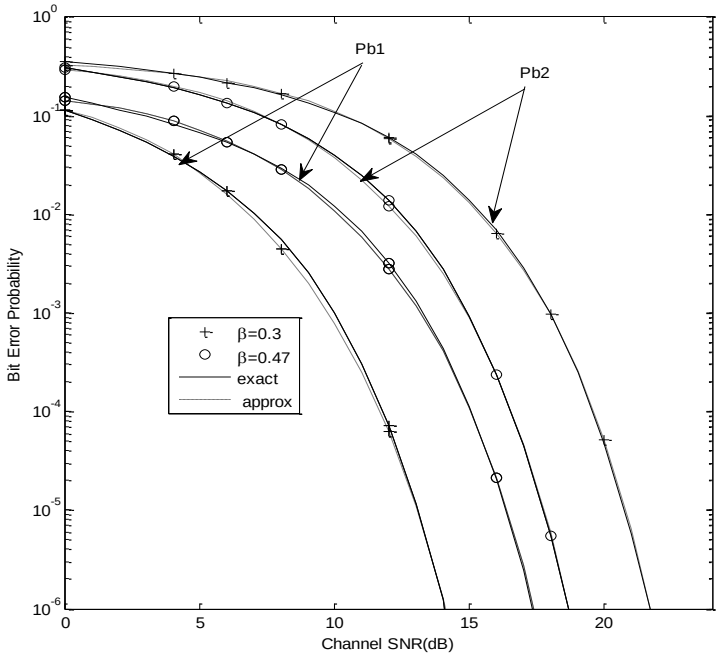

Figure 11: Exact BER and Approximate BER Curves for 4-PSK Using Exponential Function Approximation

Table 9. Polynomial Coefficients for 4-PSK Using Exponential Function Approximation

i		p_3	p_2	p_1	p_0
1	$a_\beta^{(1)}$	-0.728	0.718	-0.162	0.054
	$b_\beta^{(1)}$	1.609	0.169	-2.166	1.013
	$c_\beta^{(1)}$	-6.678	8.191	-3.578	0.706
2	$a_\beta^{(2)}$	-7.336	6.727	-1.916	0.306
	$b_\beta^{(2)}$	-1.284	1.434	-0.059	0.003
	$c_\beta^{(2)}$	3.831	-3.034	0.718	0.185

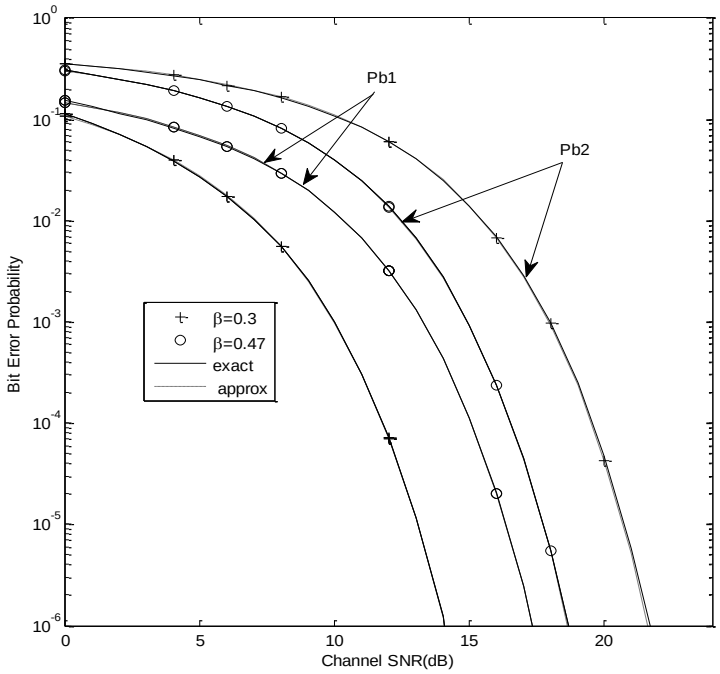

Figure 12: Exact BER and Approximate BER Curves for 4-PSK Using Complementary Error Function Approximation

Table 10. Polynomial Coefficients for 4-PSK Using Complementary Error Function Approximation

i		p_3	p_2	p_1	p_0
1	$a_\beta^{(1)}$	-0.779	0.860	-0.311	0.284
	$b_\beta^{(1)}$	0.996	0.751	-2.329	1.02
	$c_\beta^{(1)}$	-21.859	26.731	-11.238	1.698
2	$a_\beta^{(2)}$	30.936	-32.444	10.826	-0.639
	$b_\beta^{(2)}$	0.809	-0.643	0.574	-0.059
	$c_\beta^{(2)}$	-31.680	33.738	-11.331	1.197

Further comparison of the approximation Equation (15) and (16) is done by plotting the average BER probability for 4-PSK. The average BER probability ($\bar{P}_b$) for 4-PSK is given by Equation (22). Figures 13 and 14 show the average BER probability along with their respective polynomial coefficient in Tables 11 and 12. Average BER probability ($\bar{P}_b$) for 4-PSK is given by:

$$\bar{P}_b = \frac{P_b^{(1)} + P_b^{(2)}}{2} \tag{22}$$

Again by inspecting the results for the average BER probability for 4-PSK, it is seen that the complementary error function produces better curve fit as compared to exponential function for both average and individual BER probability.

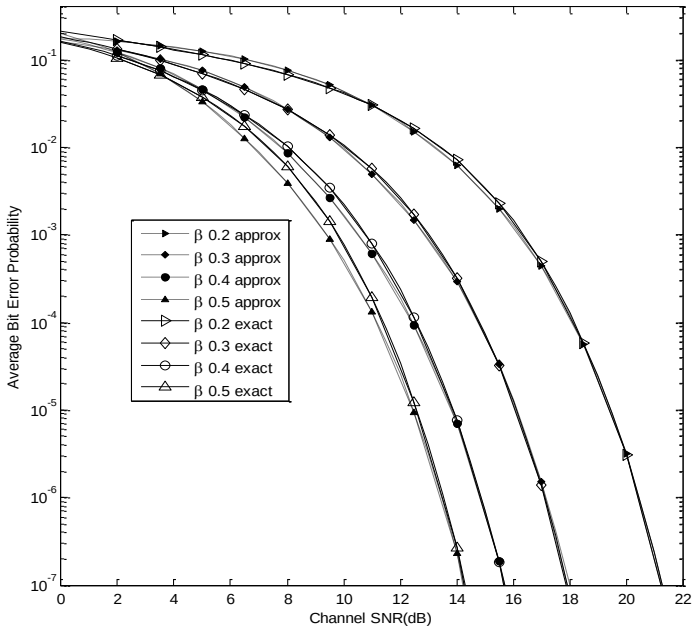

Figure 13: Exact Average BER and Approximate Average BER Curves for 4 PSK Using Exponential Function Approximation

Table 11. Average BER Polynomial Coefficients for 4-PSK Using Exponential Function Approximation

	p_3	p_2	p_1	p_0
a_β	-7.503	6.986	-2.014	0.120
b_β	-2.087	3.309	-0.143	0.012
c_β	-9.693	13.048	-4.431	0.590

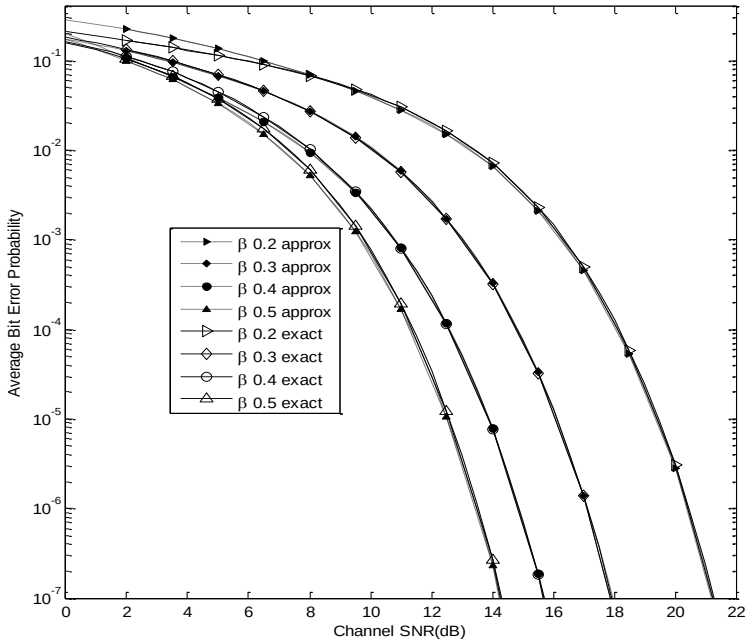

Figure 14: Exact Average BER and Approximated Average BER Curves for 4-PSK Using Complementary Error Function Approximation

Table 12. Average BER Polynomial Coefficients for 4-PSK Using Complementary Error Function Approximation

	p_3	p_2	p_1	p_0
a_β	21.037	-17.680	4.766	-0.159
b_β	-2.147	3.375	-0.170	0.0115
c_β	-257.523	258.513	-75.202	6.731

2.2.6 Probability of Bit Error 8-PSK

8-PSK results are shown in Figures 15-18 for the average BER and exact BER probability for both approximation expressions i.e. Equations (15) and (16). Again these results shown below are in agreement with our finding for 16-QAM, 64-QAM, and 4-PSK that complementary error function approximation expression bit-error rate produces better curve fitting result as compared to the exponential function. The comparison validates the appropriateness and the validity of the complementary error function BER approximation equation for our intended purpose.

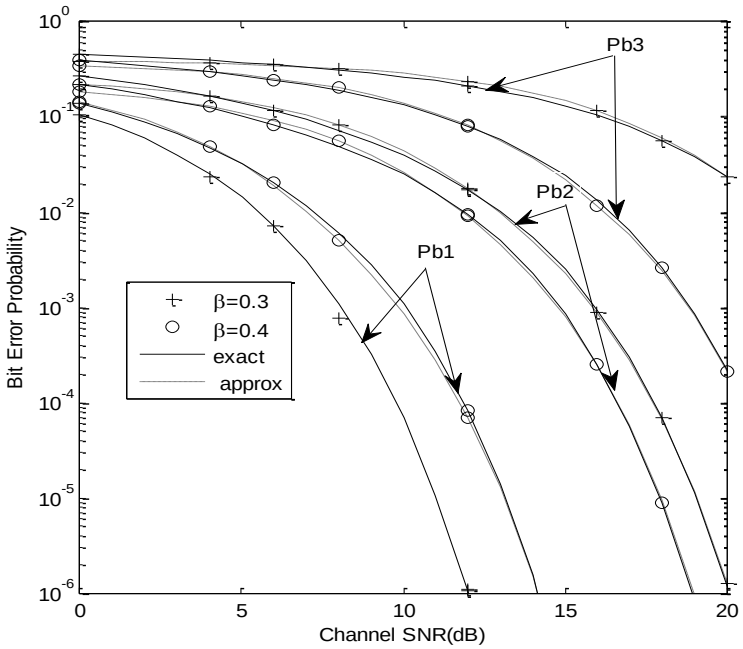

Figure 15: Exact BER and Approximate BER Curves for 8-PSK Using Exponential Function

Table 13. Polynomial Coefficients for 8-PSK Using Exponential Function Approximation

		p_3	p_2	p_1	p_0
1	$a_\beta^{(1)}$	-0.305	0.8627	-0.457	0.115
	$b_\beta^{(1)}$	7.733	-9.708	1.353	0.931
	$c_\beta^{(1)}$	22.811	-22.758	5.615	0.186
2	$a_\beta^{(2)}$	-3.231	3.493	-1.212	0.198
	$b_\beta^{(2)}$	-1.807	1.079	0.235	-0.011
	$c_\beta^{(2)}$	3.330	-2.826	0.382	0.252
3	$a_\beta^{(3)}$	1.714	0.010	-0.918	0.392
	$b_\beta^{(3)}$	2.919	-1.218	0.208	-0.011
	$c_\beta^{(3)}$	-1.182	0.598	0.155	0.167

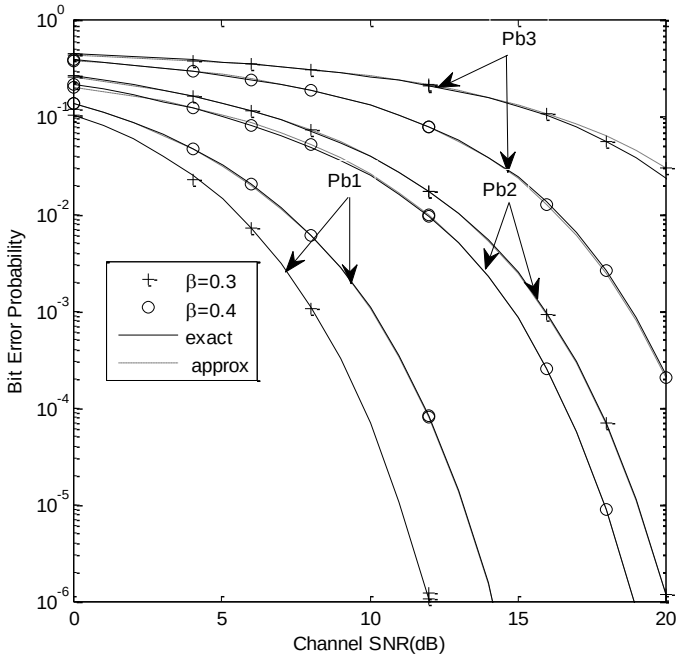

Figure 16: Exact BER and Approximate BER Curves for 8-PSK Using Complementary Error Function Approximation

Table 14. Polynomial Coefficients for 8-PSK Using Complementary Error Function Approximation

		p_3	p_2	p_1	p_0
1	$a_\beta^{(1)}$	-3.364	5.127	-2.628	0.696
	$b_\beta^{(1)}$	7.820	-9.774	1.373	0.923
	$c_\beta^{(1)}$	105.312	-113.186	35.166	-2.330
2	$a_\beta^{(2)}$	-11.875	12.929	-4.500	0.739
	$b_\beta^{(2)}$	-1.821	1.124	0.202	-0.008
	$c_\beta^{(2)}$	22.711	-23.929	7.314	-0.397
3	$a_\beta^{(3)}$	-33.759	34.583	-10.217	1.206
	$b_\beta^{(3)}$	1.354	0.264	-0.210	0.018
	$c_\beta^{(3)}$	33.068	-34.078	10.224	-0.699

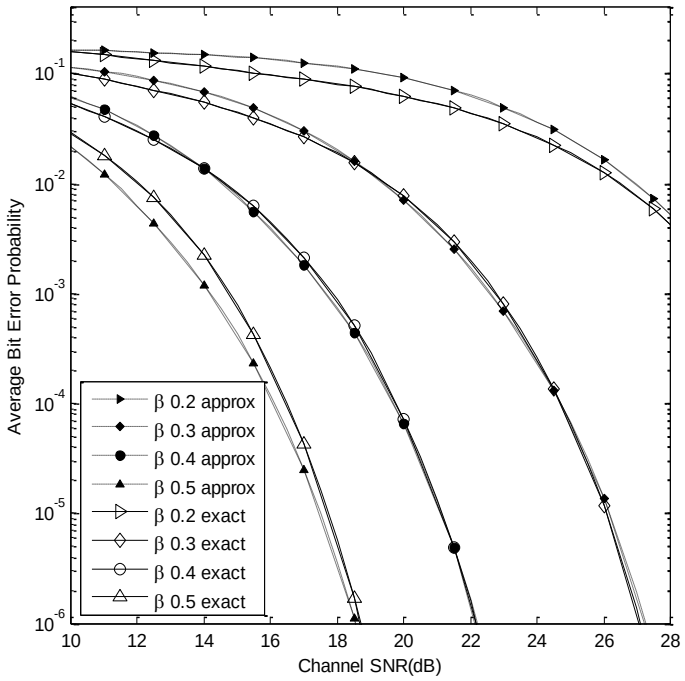

Figure 17: Exact Average BER and Approximate Average BER Curves for 8-PSK Using Exponential Function Approximation

Table 15. Average BER Polynomial Coefficients for 8-PSK Using Exponential Function Approximation

	p_3	p_2	p_1	p_0
a_β	-5.083	6.312	-2.467	0.339
b_β	2.483	-0.799	0.080	000
c_β	9.819	-8.681	2.616	-0.135

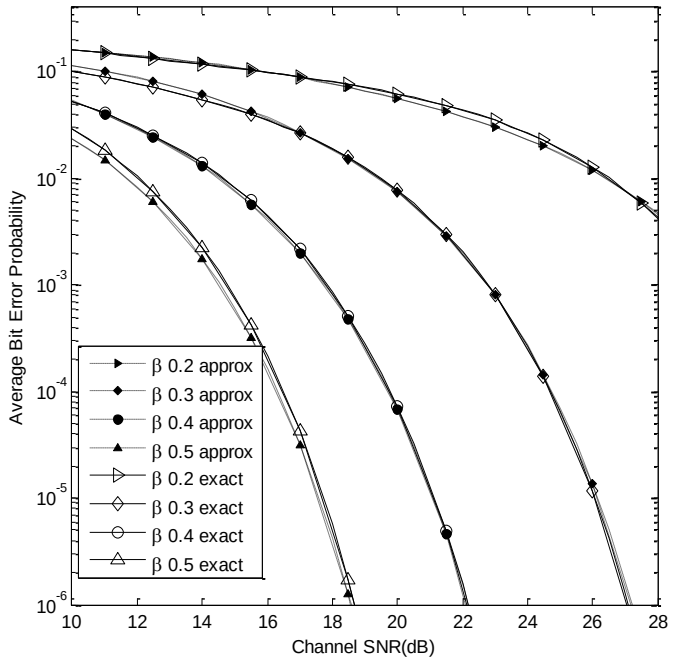

Figure 18: Exact Average BER and Approximate Average BER Curves for 8-PSK Using Complementary Error Function Approximation

Table 16. Average BER Polynomial Coefficients for 8-PSK Using Complementary Error Function Approximation

	p_3	p_2	p_1	p_0
a_β	21.445	-19.959	6.149	-0.489
b_β	2.983	-1.354	0.268	-0.019
c_β	-19.286	19.243	-5.895	0.701

2.2.7 Optimum Beta Value

In order to determine the optimum phase offset ratio or constellation shape parameter (β) value for each modulation scheme, the beta (β) value that results into the minimum of the maximum CNR (γ_{req}^{i}) needs to be determined. Obtaining the optimum β value for different modulation scheme ensures that each modulation scheme maximizes its capability based on the specified quality of service QoS.

In the adaptive modulation scheme designed in this research, bits from each distinct class are assigned to a specific bit position of an asymmetric 64-QAM constellation that is matched to the prescribed BER requirements. The optimal beta (β) leads to modulation embedding gain and facilitate multimedia data with different BER requirements. The algorithm determines the beta value that results in the minimum of the maximum CNR.

For the particular case of 4/16 QAM

$$\arg \min_{\beta} \{ \max_{i} \{ \gamma_{reg}^{(i)} \} \}$$

Example of specified QoS is:

$$\text{s.t } P_b^{(1)} \leq 10^{-5}$$

$$P_b^{(2)} \leq 10^{-5}$$

$$P_b^{(3)} \leq 10^{-3}$$

$$\beta \in (0,0.5], i \in \{1,2,3\}$$

An example for obtaining the optimum beta value will be demonstrated in Chapter 3.

It is important to note that the exact BER expression in Section 2.1.3 is not easily invertible with respect to CNR (γ_{req}^{i}); hence the reason why Equation (16) was developed

in Section 2.2.1. Inverting Equation (16) in terms of CNR (γ_{req}^{i}) result into Equation (23). Equation (24) from Annamalai et al [2] and Equation (23) are the complementary error function and exponential function approximation BER equations, respectively, in terms of CNR (γ_{req}^{i}). Using the exact BER expressions for the different modulation schemes, the required CNR for specified quality of service can be found. This is done by manually plotting the BER curve and finding the threshold values through graphical tool. However, the manual method is labor intensive and cannot be automated. The invertible expression provides a quick and easy method to determine the required CNR for the specified quality of service (QoS).

$$\gamma_{req}^{(i)}(\beta) = -\frac{1}{b_{\beta}^{(i)}} erfcinv\left[-a_{\beta}^{(i)} + \frac{\sqrt{(a_{\beta}^{(i)})^2 + 4c_{\beta}^{(i)} P_b^{(i)}}}{2c_{\beta}^{(i)}} \right]^2 \tag{23}$$

$$\gamma_{req}^{(i)}(\beta) = -\frac{1}{b_{\beta}^{(i)}} \ln\left[-a_{\beta}^{(i)} + \frac{\sqrt{(a_{\beta}^{(i)})^2 + 4c_{\beta}^{(i)} P_b^{(i)}}}{2c_{\beta}^{(i)}} \right] \tag{24}$$

where i= 1, 2, 3... $\log_2 M$.

2.2.8 Remarks

Tables 1- 16 summarize the values of polynomial coefficients $a_{\beta}^{(1)}$ $b_{\beta}^{(2)}$ and $c_{\beta}^{(3)}$ for 4-PSK, 16-QAM, and 64-QAM and 8-PSK modulation. These values were obtained by curve-fitting a sufficiently large number of data points from the exact BER expressions to the approximate BER formula using a Quasi-Newton unconstrained optimization method. After comparing the results, the complementary error function approximation demonstrated better curve fit. The complimentary error function approximation does not only show better curve fitting result but it also produces better

result when finding the required CNR given distinct BER requirement in the proposed receiver oriented rate adaptation strategy and adaptive multi-resolution modulation scheme. The complementary error function approximation validates the exact BER probability and was use to approximate the exact BER equation in order to automatically make decision on thresholds for different modulation schemes based on the required QoS and channel conditions.

Table 17 confirms that the complementary error function (erfc) approximation is better than exponential function approximation. Table 17 shows a comparison of results obtained for predicting the required CNR γ_{reg} using exponential and erfc approximation.

Table 17. Comparison of Exponential and Complementary Error Function Approximation

Modulation scheme		4PSK	8-PSK	16QAM	64QAM
Optimum Beta (β)		0.4	0.43	0.43	0.42
Exact (graphical) (γ_{req})		11.4	23.35	17.86	25.32
Exponential	γ_{req}	11.43	23.12	17.75	25.13
	% error	0.263	0.985	0.985	0.750
ERFC	γ_{req}	11.43	23.27	17.90	25.49
	% error	0.263	0.343	0.343	0.671

The result from Table 17 solidifies the author's claim that the complementary error function approximation produces better curve fitting result. The table reveals that for a specified QoS, the CNR for the erfc is closer to the exact CNR value as compared to the exponential function. The percentage error for ercf approximation is smaller than that for exponential function approximation. It is worth noting that although the percentage error difference between the two approximations may seem small in decibel (dB) value, but when normalized, this difference magnify to a significant gain.

3.0 RECEIVER-ORIENTED RATE ADAPTATION

3.1 Method and Assumptions

The receiver-oriented rate adaptation done by Annamalai et al [2] used phase-shift keying (PSK) modulation scheme. However, in this project quadrature amplitude modulation (QAM) is employed. QAM has the functionality of increasing the efficiency of transmission for wireless radio communications systems in local area network (LAN) by utilizing both amplitude and phase variations. The use of PSK is applied to long distance communication such as satellite [2]. The results from Annamalai et al [2] reveals that the ABER and spectral efficiency plot reveal that the proposed receiver-oriented rate-adaptation scheme achieves a much higher effective bit rate as compared to the conventional QPSK system while facilitating multimedia data transmission. In this project, QAM is applied to obtain similar result that can be useful to LAN.

This chapter illustrates that it is possible to achieve better spectral utilization efficiency by recovering the correctly received bits with a higher probability within erroneously received symbols. This is realized without engaging the higher layer protocols especially at low and moderate values of the channel carrier-to-noise ratios. In the receiver-oriented rate adaptation scheme, the transmitter is operating at a constant power and signaling rate, but the receiver adapts its demodulation scheme according to the prevailing channel conditions that is based on the CSI available at the each receiver. For example, when the carrier-to-noise ratio (CNR) falls between two specified threshold values γ_{T2} and γ_{T3}, the receiver will demodulate the transmitted 64-QAM symbol as 16-QAM symbol since 16-QAM constellation is embedded within the 64-QAM signal constellation as shown in Figure 1. Hence recovering the two most significant bit-classes

out of the three bit-classes which were transmitted i.e. four bits. It is worth noting that recovering of the two most significant bit-classes is achieved for the same transmission power and the smaller size constellation creates a larger Euclidean distance between the signal points. This provides better immunity against channel fading and noise. Figure 19 shows the block diagram of the proposed receiver-oriented rate adaptation.

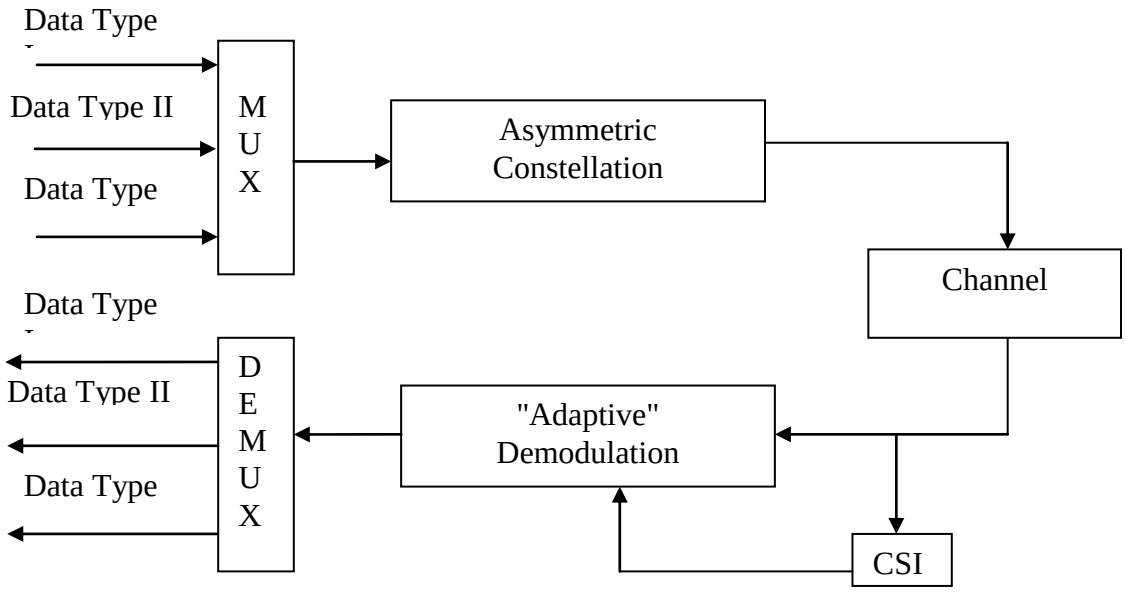

Figure 19: Receiver-oriented Rate Adaptation-rates

The term “adaptive symbol demodulation” in Figure 19 does not indicate that different demodulators at different CNR regions are being utilized. This term was introduced for establishing the decision regions needed in the assessment of exact bit error probability for each bit-class in the signal constellation. For the implementation of the receiver, only an asymmetric 64-QAM symbol demodulator would be needed. If the received CNR is above γ_{T3} , all six detected bits would be retained. If the received CNR is the range

$[\gamma_{T2}, \gamma_{T3})$ the four most significant bits would be retained, $[\gamma_{T1}, \gamma_{T2})$ only the two MSB would be retained. Below γ_{T1} then all bits would be dropped. The thresholds γ_{T1}, γ_{T2} and γ_{T3} are selected to meet the particular QoS requirements for each bit in the signal constellation. The choice of which bits should be dropped to sustain the wireless link quality at a desired level is dependent on the selection of Gray code bit mapping for the signal points.

It is important to recognize the duality between the problems of finding the optimal signaling strategy in our case with that of signaling in broadcast/multicast channels. The sender sends multiplexed multimedia data via multicast constellation which is matched to the user quality of service (QoS) requirements in our passive rate adaptation scheme. The distinct demodulation state at the receiver corresponds to channels with different capacities in terms of the broadcast/multicast channel analogy. However, in this scheme only one channel is active to convey data at any given time. This active channel is called virtual broadcast channel, regardless if they are all sharing the same physical medium. This validates the selection of a multi-resolution modulation scheme to represent the source compactly in a hierarchy of resolutions in our proposed passive rate adaptation problem. Another feature of the scheme proposed in this work is that it allows for graceful signaling rate reduction in LAN. Whenever the channel condition worsens for a short period of time, link outage will not be declared. Link outage requires the search for a new route path and in the process causes considerable delay and overhead. The proposed scheme avoids this costly rerouting to establish a new link. In so doing the wireless link quality is maintained at the desired level without engaging the higher layer protocols or the dynamically adapting transmission parameters

at the transmitter. Furthermore, the scheme may provide an additional degree of rate control when it is used in tandem with the more sophisticated transmitter-oriented rate adaptation mechanisms examined by Pursley et al [9] and Hossain et al [10].

3.2. Procedure: Adaptive Receiver

One of the goals of the passive rate adaptation scheme is to reduce the signaling rate at the receiver. This is done by adaptively demodulating the embedded constellation according to the channel condition to maintain the link quality at a wanted level. In so doing, the receiver is able to still recover some of the transmitted bits correctly regardless if a symbol has been received in error. In the conventional scheme this adaptation is not permitted and it is sensible to presume that all bits will be dropped for failing to meet the specified link BER requirement. For this reason the spectral efficiency can be expected to improve with this scheme compared to the conventional non-adaptive scheme.

3.2.1 Steady-state Probabilities of Discrete Markov Chains

In an asymmetric 64-QAM, there are three information bit- classes associated with each of the symbol if M=8. Since $\log_2 8=3$, there are three states corresponding to the different receiver demodulation: state G, state M and state B. When the condition is very bad, state B as shown in Figure 20, the receiver attempts to demodulate only the first bit. In state G, the receiver attempts to recover all the transmitted bits. Given a set of instantaneous BER requirements, the minimum required CNR/symbol $\gamma_1, \gamma_2, \gamma_3$ that is associated with each bit class of an asymmetric 64-QAM symbol that satisfy the QoS constraints can be determine, by using Equation (2.24). It is worth mentioning that using the asymmetric constellation; the data bit stream with the most stringent BER requirement is mapped into the most significant bit position of the M-ary asymmetric

constellation at the transmitter. However, threshold channel CNRs (i.e., that will dictate which bit should be dropped after the demodulation operation so as to maintain the specified link quality in a randomly fluctuating condition) are not identical to these target CNRs but they are related as follows:

$$\gamma_{T1} = \gamma_1^*, \quad \gamma_{T2} = \max(\gamma_1^*, \gamma_2^*), \quad \gamma_{T3} = \max(\gamma_1^*, \gamma_2^*, \gamma_3^*)$$

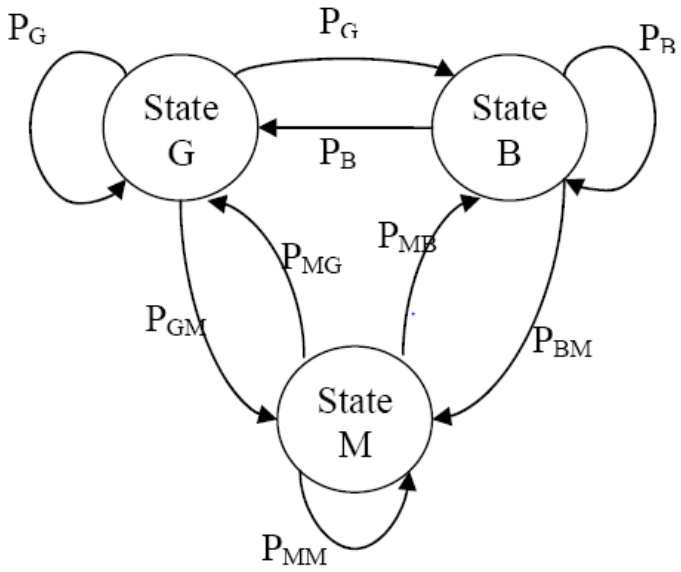

Figure 20: A 3-state Discrete Markov Chain for Modeling the Multicast 8-PSK Receiver Demodulation Operation

In order to determine which state is reached by the receiver, the following decision rules are employed:

- If $\gamma > \gamma_{T3}$, the receiver demodulate the received signal as an asymmetric 64-QAM
- If $\gamma_{T2} < \gamma > \gamma_{T3}$, the receiver demodulates the received signal as an asymmetric 16-QAM waveform (state M).
- $\gamma_{T1} < \gamma > \gamma_{T2}$, receiver demodulates the received signal as a 4-QAM waveform (State B).

- $\gamma < \gamma_{T1}$, the receiver is unable to recover any bits correctly, hence it will drop all three bit class (6 bits) since the prescribed link quality (BER) cannot be sustained.

where γ denotes the symbol carrier-to-noise ratio and its cumulative distribution function (CDF) is given by $F_\gamma(\gamma)$.

The state transition probabilities for the above example of 3-state discrete Markov chain can be expressed compactly using the transition probability matrix P,

$$\mathbf{P} = \begin{bmatrix} \mathrm{P_{GG}} & \mathrm{P_{GM}} & \mathrm{P_{GB}} \\ \mathrm{P_{MG}} & \mathrm{P_{MM}} & \mathrm{P_{MB}} \\ \mathrm{P_{BG}} & \mathrm{P_{BM}} & \mathrm{P_{BB}} \end{bmatrix} = \begin{bmatrix} 1-F_\gamma(\gamma_{T3}) & F_\gamma(\gamma_{T3})-F_\gamma(\gamma_{T2}) & F_\gamma(\gamma_{T2})-F_\gamma(\gamma_{T1}) \\ 1-F_\gamma(\gamma_{T3}) & F_\gamma(\gamma_{T3})-F_\gamma(\gamma_{T2}) & F_\gamma(\gamma_{T2})-F_\gamma(\gamma_{T1}) \\ 1-F_\gamma(\gamma_{T3}) & F_\gamma(\gamma_{T3})-F_\gamma(\gamma_{T2}) & F_\gamma(\gamma_{T2})-F_\gamma(\gamma_{T1}) \end{bmatrix} \quad 25)$$

The steady state probabilities may be found as $\mathrm{P}^\infty = \mathrm{P}$ which simplifies into the following intuitive result:

$$P_G = 1-F_\gamma(\gamma_{T3}),\ P_M = F_\gamma(\gamma_{T3})-F_\gamma(\gamma_{T2}),\ P_B = F_\gamma(\gamma_{T2})-F_\gamma(\gamma_{T1}) \qquad (26)$$

3.2.2 Average Probabilities of Bit Error

The average probability of bit error (ABER) in AWGN channel is the weighted sum of the average bit error probability in the each of the Markov states and is given by

$$P_b = P_G\left[\frac{P_b^{(1)}(\gamma_s)+P_b^{(2)}(\gamma_s)+P_b^{(3)}(\gamma_s)}{3}\right] + P_M\left[\frac{P_b^{(1)}(\gamma_s)+P_b^{(2)}(\gamma_s)}{2}\right] + P_B P_b^{(1)}(\gamma_s) \qquad (27)$$

Where $P_b^{(i)}(\gamma_s)$ denotes the BER of the i-th bit in an AWGN channel. In a multipath flat-fading channel, the ABER can be computed as

$$\overline{P_b} = \left[1-F_\gamma(\gamma_3)\right]\int_0^\infty \left[\frac{P_b^{(1)}(\gamma_s)+P_b^{(2)}(\gamma_s)+P_b^{(3)}(\gamma_s)}{3}\right] f_{\gamma_s}(\gamma_s)d\gamma_s$$

$$+\left[F_\gamma(\gamma_3)-F_\gamma(\gamma_2)\right]\int_0^\infty\left[\frac{P_b^{(1)}(\gamma_s)+P_b^{(2)}(\gamma_s)}{2}\right]f_{\gamma_s}(\gamma_s)d\gamma_s \tag{28}$$

$$+F_\gamma(\gamma_2)\int_0^\infty P_b^{(1)}(\gamma_s)\ f_{\gamma_s}(\gamma_s)d\gamma_s$$

This equation can be evaluated efficiently using a frequency domain analysis technique such as the moment generating function (MGF) method or the characteristic function (CHF) method for generalized fading channels.

3.2.3 Effective Bit Rate

Figure 21 shows the exact BER performance for each bit-class in the asymmetric 64-QAM constellation over an AWGN channel. When $\beta = 0.5$, the performance curves correspond to the "traditional" symmetrical 64-QAM modulation. From the plot, it can be seen that when $\beta = 0.3$, the BER of the first bit is better than both conventional 16 and 64-QAM.

If symmetric is employed 64-QAM modulation, the received channel CNR of 22.5 dB is required to recover all the three bit-class correctly in order to satisfy QoS requirement of 10^{-3}. However, employing non-uniform 64-QAM, the receiver can recover the first bit-class correctly (i.e., satisfying the QoS constraint) with less energy. The figure also reveals that asymmetric constellation can be used to support multi-service QoS data transmission. This is demonstrated by the example shown with Table 18.

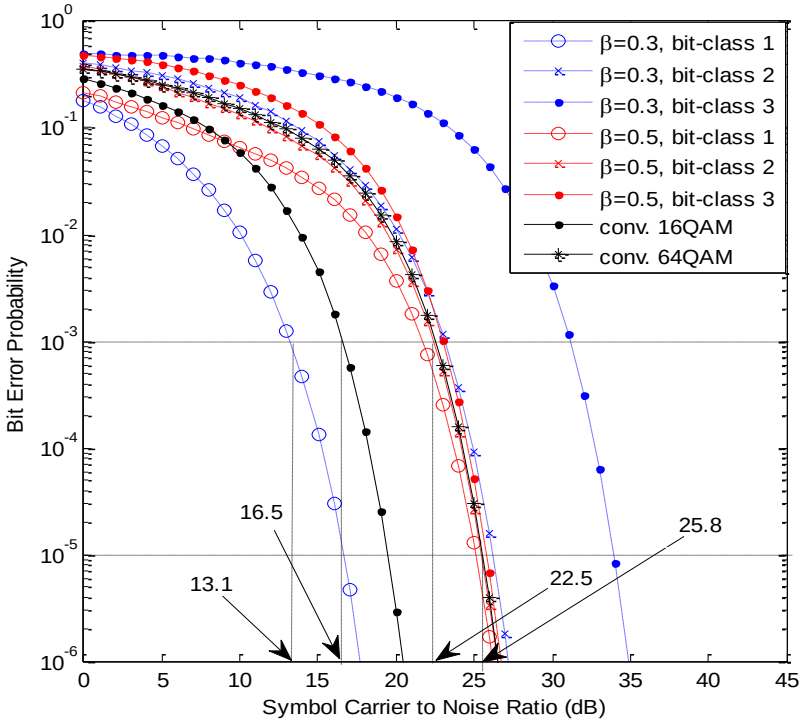

Figure 21: Bit Error Probabilities of Asymmetric 64-QAM

If three binary data streams with non-identical BER requirements of 10^{-5}, 10^{-4} and 10^{-3} are needed to send data from a wireless router to a laptop in a local area network using 64-QAM modulation scheme. In the "conventional" system, the data is assumed to be multiplexed and would be transmitted by symbols in a uniformly spaced 64-QAM constellation. The required CNR/symbol must be chosen to satisfy the most stringent QoS requirement of 10^{-5} which is about 25.803 dB (the CNR that satisfies QoS of 10^{-5} for the third bit class for the conventional scheme) for recovering the three bit classes in conventional scheme. Whereas in the proposed scheme, asymmetric 64-QAM constellation is employed and appropriately map the data streams such that the first bit, has BER requirement of 10^{-5}, the second bit has a BER requirement for 10^{-4} and the third bit must satisfy the BER requirement for 10^{-3}. Using the algorithm developed in Section

2.2.7, it is evident from Table 18 that the optimum phase offset ratio (β) is 0.48 and the BER requirements for all three classes of data can be satisfied with CNR/symbol of 24.081 dB, resulting in embedding gain of 1.72 dB.

Table 18. Threshold CNR for Several Beta Values 64-QAM

β	γ_1^* (dB)	γ_2^* (dB)	γ_3^* (dB)	max γ^* (dB)
0.12	13.440	30.555	46.673	46.673
0.20	14.531	27.068	37.929	37.929
0.25	15.447	25.782	34.147	34.147
0.35	18.031	24.374	28.571	28.571
0.42	20.594	24.059	25.666	25.666
0.43	21.062	24.048	25.298	25.298
0.44	21.516	24.045	24.961	24.961
0.45	22.043	24.050	24.592	24.592
0.46	22.556	24.062	24.259	24.259
0.47	23.141	24.081	23.948	24.081
0.48	23.748	24.108	23.609	24.108
0.49	24.401	24.143	23.301	24.401
0.50	25.129	24.185	23.020	25.129

One of the key features that should be noted with the propose receiver-oriented adaptive rate scheme is that symbol may be received incorrectly; however unlike conventional scheme the receiver-oriented adaptive rate scheme can retain or recover the classes or class of bits that may have been received correctly instead of discarding all the bits within the symbol. The framework to quantify the improvement in spectral utilization efficiency is developed.

Let us define the effective bit rate (in terms of bits/Hz) as

$$R_{eff} = P_\gamma(\gamma < \gamma_{TI})(0) + P_\gamma(\gamma_{T1} < \gamma < \gamma_{T2})(1) + P_\gamma(\gamma_{T2} < \gamma < \gamma_{T3})(2) + P_\gamma(\gamma < \gamma_{T3})(3) \quad (29)$$

Where $P_{\gamma_s}(\gamma_s < \gamma_T) = F_{\gamma_s}(\gamma_T)$ which leads to,

$$R_{eff} = (F_\gamma(\gamma_{T1}))(0) + (F_\gamma(\gamma_{T2}) - F_\gamma(\gamma_{T1}))(1) + (F_\gamma(\gamma_{T3}) - (F_\gamma(\gamma_{T2}))(2) + (1 - F_\gamma(\gamma_{T3}))(3) \quad (30)$$

In a Rayleigh fading channel, the corresponding CDF is given by $F_{\gamma_s}(\gamma_s) = 1 - e^{-\frac{\gamma_s}{\Omega}}$, where Ω denotes the mean channel CNR/symbol, i.e., $\Omega = \overline{E_s}/N_o$. Substituting this CDF in Equation (30), a very simple expression for the effective bit rate in a Rayleigh fading channel is obtained as

$$R_{eff} = e^{-\frac{\gamma_{T1}}{\Omega}} + e^{-\frac{\gamma_{T2}}{\Omega}} + e^{-\frac{\gamma_{T3}}{\Omega}} \tag{31}$$

Table 18 lists the target CNR/symbol values ($\gamma_1^*, \gamma_2^*, \gamma_3^*$) for different phase offset ratios which satisfy the BER constraints of [10^{-5} 10^{-4} 10^{-3}].

3.3 Results and Discussion

Figure 22 shows the spectral efficiency of 16-QAM where the optimum constellation design is matched to the unequal QoS requirements of 10^{-5} and 10^{-3}. Figure 23 illustrates the spectral efficiency of 64-QAM at the optimum constellation design that matches to the unequal QoS requirements of 10^{-5}, 10^{-4} and 10^{-3}. The optimum value of beta for both cases is 0.43, and 0.5 is the conventional uniform constellation for 16 and 64 QAM. Both of these figures disclose that the proposed receiver-oriented rate-adaptation scheme achieves a much higher effective bit rate at the optimum beta value as compared to the conventional system while facilitating multimedia transmission. Figure 24 depicts the average probability bit error rate (ABER) performance of the adaptive system for 16 and 64 QAM. While there was much higher effective bit rate for the spectral efficiency plot, the ABER attained is slightly worse than conventional system. This spectral efficiency gain is attained by slightly sacrificing the ABER performance at higher mean CNR/symbol values.

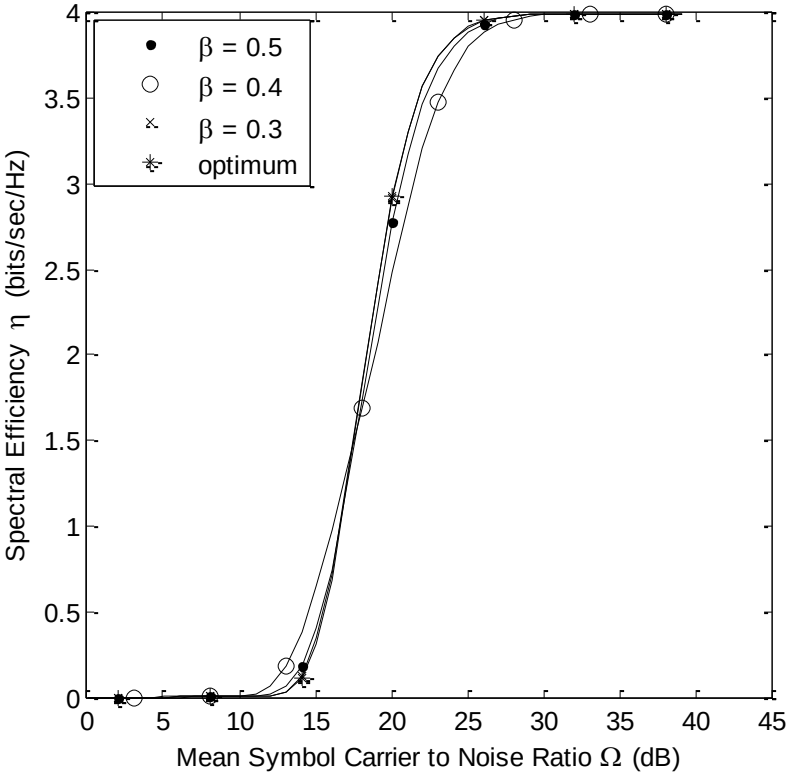

Figure 22: Spectral Efficiency of 16-QAM for Broadcast Channel With QoS of 10^{-5} and 10^{-3} Under Nakagami-m (m=3)

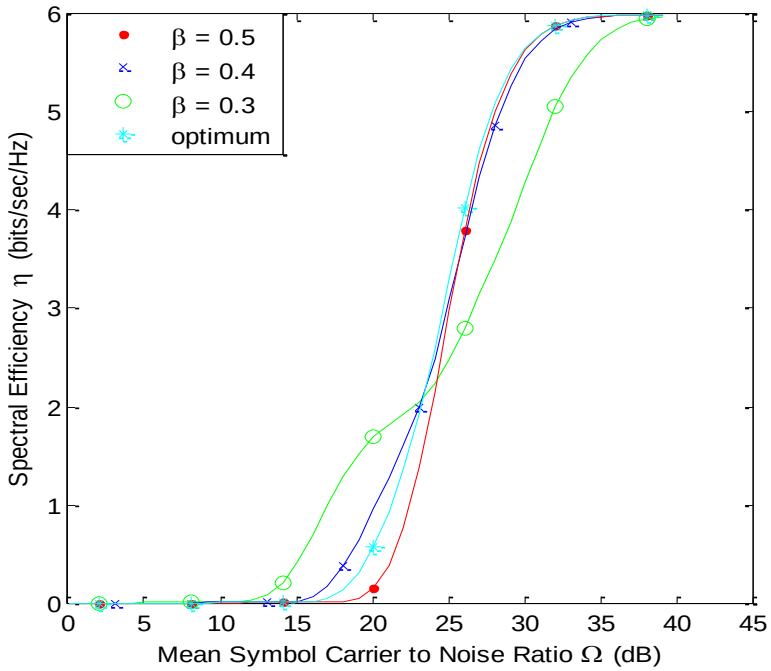

Figure 23: Spectral Efficiency of 64-QAM for Broadcast Channel With QoS of 10^{-5}, 10^{-5} and 10^{-3} Under Nakagami-m (m=3)

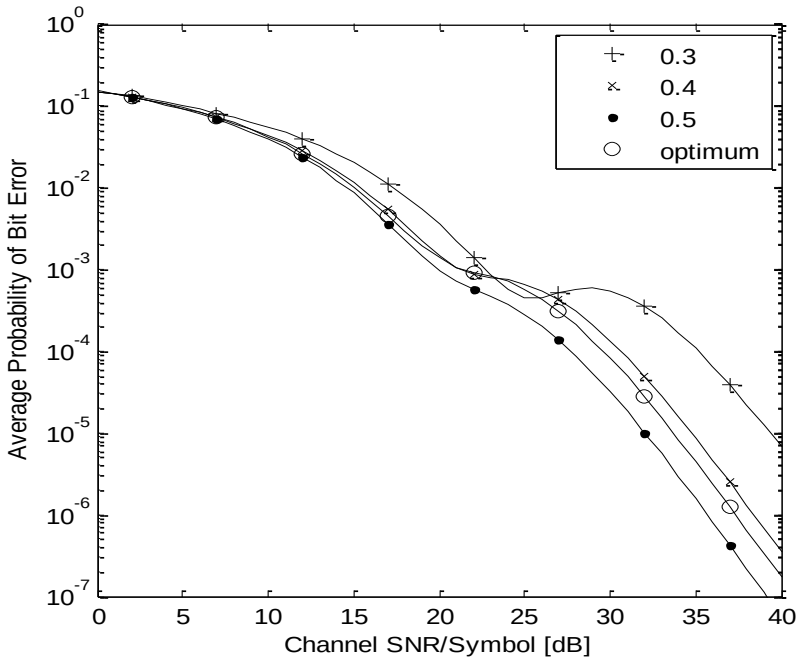

Figure 24: Average Probability of Bit Error for 64-QAM Under Nakagami-m Channel (m=3)

The following briefly describe the behavior of the proposed receiver-oriented adaptive rate scheme at different regions of the average channel CNR/symbol for 64-QAM:

Case 1: 0 - 10dB

In extremely poor channel conditions, (i.e. the range of 0-10 dB), it is observed that the scheme has a very small spectral efficiency gain over conventional scheme. However for the ABER, the conventional scheme is slightly better than the scheme proposed in this work.

Case 2: 10 - 20dB

In this range the spectral efficiency for the scheme has increased significantly as compared to conventional 64-QAM. The ABER for the scheme is getting worse than conventional scheme.

Case 3: 20dB - 40dB

In a better fading channel conditions (i.e. 20-40dB), it is noticed that the ABER of the proposed passive rate adaptation scheme with nonuniform constellation performs slightly worse than the conventional symmetric 64-QAM constellation. However, it should be emphasized that the energy efficiency improvement still persists as the designed scheme have an “optimal” waveform that is matched to the unequal error protection requirements for different classes of data.

4.0 ADAPTIVE MULTI-RESOLUTION MODULATION

Annamalai et al [2, 3] have demonstrated that for a constant signaling rate i.e. fixed signal constellation size; the shape of an asymmetric PSK can be designed to match the unequal error protection (UEP) requirement for different classes of traffic types. Whenever the channel condition fluctuates over a wide range, adapting the shape of the constellation may not be adequate to achieve a high throughput. Because of this reason, this research considers the designing of hierarchical adaptive modulation that can support multimedia traffic over generalized multipath fading channel for using M-ary QAM.

4.1 Method

Like in [20], we consider a circumstance whereby the channel necessitates maintaining two different types of traffic demanding two different QoS. The given qualities of service are 10^{-5} and 10^{-3}. Depending on the channel condition, the scheme should be able to decide the best modulation scheme to employ in order to meet the required QoS. There are two methods by which the scheme decides the best modulation scheme. The first method is the labor-intensive method. That is plotting the curve using the exact equation, and manually establishing the threshold values through graphical analysis for different modulation schemes. The second method is utilizing the invertible expression in Chapter 2 (Equation (16)) to predict the CNR (γ_{REQ}). The manual technique is rigorous, time consuming and cannot be automated. Therefore, the invertible expression provides an extremely straightforward and simple approach for determining the threshold values. The exact equation for the bit error rate is not readily invertible with respect to its symbol CNR; hence the reason for developing the complementary error function BER approximation in Section 2.2.1 Equation (16).

For the conventional scheme, the threshold values were determined using the most stringent condition which is QoS of 10^{-5}. However for the adaptive multi-resolution scheme, the required QoS for the average BER is the average of the individual QoS. Table 19 demonstrates the calculations for the different modulation classes considered in this work. Figure 25 illustrates the threshold value determination for both the conventional scheme and the adaptive multi-resolution scheme using the manual method. The plot is for the case where phase offset ratio α, β=0.5. As mentioned, above the manual method is rigorous and cannot be automated.

Table 19. Illustrate the Calculations for the Different Modulation Classes Considered

For (4PSK, 16QAM)	For (64QAM)
$P_b^{(1)} \le 10^{-5}$ $P_b^{(2)} \le 10^{-3}$ $b \in [0, 0.5]$	$P_b^{(1)} \le 10^{-5}$ $P_b^{(2)} \le 10^{-5}$ $P_b^{(2)} \le 10^{-3}$ $b \in [0, 0.5]$
$ABER_{req} = \frac{10^{-5} + 10^{-3}}{2} = 0.000505$	$ABER_{req} = \frac{10^{-5} + 10^{-5} + 10^{-3}}{3} = 0.00034$

The inter-modulation threshold values are used to determine which modulation scheme to use for different channel CNR conditions, i.e. when should different modulation schemes be employed based on the channel condition. For the adaptive multi-resolution scheme, CNR threshold values to be used to cater for each bit class in order to meet the QoS requirements for the individual bit class need to be determined. These threshold values are referred to as intra-modulation thresholds. Within each modulation scheme, the most stringent condition is assigned to the first bit and the next condition for the next bit after that. That is, 10^{-5} for bit 1 and 10^{-3} for bit 2, for the case of 4/16 QAM modulation scheme. However for the case of 4/16/64 QAM modulation scheme, 10^{-5} is assign to the bit 1, 10^{-5} for bit 2 and 10^{-3} 3 for bit 3.The optimum phase offset ratio is found by using the algorithm for optimizing β value for different modulation scheme in Section 2.2.7. As was mention in Section 2.2.7 optimizing

beta for the different modulation scheme, assures each modulation scheme exploits its potential based on the defined quantity of service.

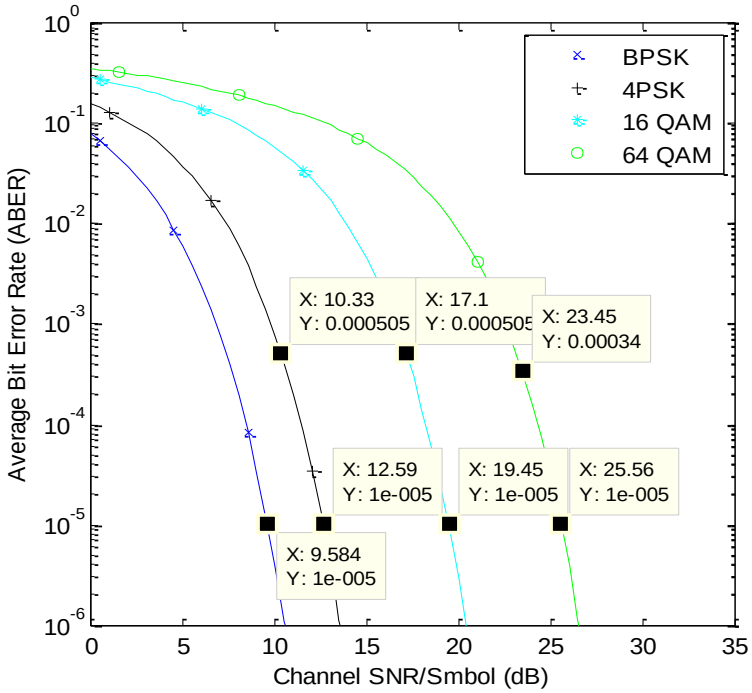

Figure 25: Threshold Value for both Conventional and Adaptive Multi-Resolution Schemes

For the adaptive multi-resolution scheme, the average spectral efficiency can be written as shown below.

$$\eta_{adap} = 1\int_{\gamma_{T1}}^{\gamma_{T2}} f_\gamma(\gamma)d\gamma + 0\int_{\gamma_{T2}}^{\gamma_{T4P_1}} f_\gamma(\gamma)d\gamma + 1\int_{\gamma_{4P_1}}^{\gamma_{T4P_2}} f_\gamma(\gamma)d\gamma + 2\int_{\gamma_{4P_1}}^{\gamma_{T4P_2}} f_\gamma(\gamma)d\gamma +$$
$$0\int_{\gamma_{T3}}^{\gamma_{16Q_1}} f_\gamma(\gamma)d\gamma + 2\int_{\gamma_{16Q_1}}^{\gamma_{16Q_2}} f_\gamma(\gamma)d\gamma + 4\int_{\gamma_{16Q_2}}^{\gamma_{T4}} f_\gamma(\gamma)d\gamma + 0\int_{\gamma_{T_4}}^{\gamma_{64Q_1}} f_\gamma(\gamma)d\gamma + \quad (32)$$
$$2\int_{\gamma_{64Q_1}}^{\gamma_{64Q_2}} f_\gamma(\gamma)d\gamma + 4\int_{\gamma_{64Q_2}}^{\gamma_{64Q_3}} f_\gamma(\gamma)d\gamma + 6\int_{\gamma_{64Q_3}}^{\gamma_\infty} f_\gamma(\gamma)d\gamma$$

Where γ_{T1}, γ_{T2}, γ_{T3}, and γ_{T4}, are the adaptive scheme's inter-modulation threshold values for BPSK, 4PSK, 16QAM and 64QAM, respectively. γ_{4P1} and γ_{4P2} are the intra modulation threshold values for 4PSK. In a similar manner, γ_{16Q1} and γ_{16Q2} are the intra modulation threshold values for 16QAM. Equation (32) is valid in a situation whereby:

$$\gamma_{T1} < \gamma_{T2} < \gamma_{4P1} < \gamma_{4P2} < \gamma_{T3} < \gamma_{16Q1} < \gamma_{16Q2} < \gamma_{T4} < \gamma_{64Q1} < \gamma_{64Q2} < \gamma_{64Q3}$$

However in a situation whereby the condition stated above is not satisfied, careful consideration should be given towards determining the appropriate spectral efficiency. A special example is the case for phase offset ratio 0.5 indicated in Table 21. The spectral efficiency will be given as:

$$\eta_{adap} = 1\int_{10^{9.58/10}}^{10^{10.33/10}} f_\gamma(\gamma)d\gamma + 0\int_{10^{10.33/10}}^{10^{12.59/10}} f_\gamma(\gamma)d\gamma + 2\int_{10^{12.59/10}}^{10^{17.1/10}} f_\gamma(\gamma)d\gamma +$$
$$0\int_{10^{17.1/10}}^{10^{19.25/10}} f_\gamma(\gamma)d\gamma + 4\int_{10^{19.25/10}}^{10^{23.45/10}} f_\gamma(\gamma)d\gamma + 0\int_{10^{23.45/10}}^{10^{25.14/10}} f_\gamma(\gamma)d\gamma + \quad (33)$$
$$2\int_{10^{25.14/10}}^{10^{25.49/10}} f_\gamma(\gamma)d\gamma + 6\int_{10^{25.49/10}}^{\gamma_\infty} f_\gamma(\gamma)d\gamma$$

4.2 Results and Discussion

Utilizing the invertible equation developed in i.e. Equation (16), various threshold values for different modulation schemes are found. With these threshold values, it is possible to estimate the spectral efficiency curve for the adaptive modulation scheme for multimedia traffic. The threshold values for the inter-modulation schemes are listed in Table 20 for QoS requirement of 10^{-5} and 10^{-3}. Also threshold values for the intra-modulation schemes are listed in Table 21. In Table 21, α (PSK) and β (QAM) are the constellation shape parameter phase offset ratio. The spectral efficiency of the system in a Nakagami-m fading channel with m = 3 is shown in Figure 26. The result shows different β values including normal transmission in which β = 0.5 and the optimum β value. From the spectral efficiency plot, the optimum beta value has highest efficiency starting from 0 dB to 40 dB as compared to the conventional scheme.

Table 20. Threshold Values for Inter-modulation Schemes (dB): QoS 10^{-5} and 10^{-3}

	BPSK	4PSK	16QAM	64QAM
Conventional Scheme	9.584	12.59	19.45	22.56
Adaptive Multi-resolution	9.584	10.33	17.1	23.45

Table 21. Threshold Values for Intra-modulation Schemes (dB):QoS 10^{-5} and 10^{-3}

Modulation	Bit Class	α, β=0.3	α, β=0.4	α, β=0.5	α, β=optimum	Optimum value
4PSK	Bit 1	10.59	11.42	12.59	11.43	0.4
	Bit 2	13.64	11.38	9.79	11.4	
16QAM	Bit 1	15.74	17.34	19.25	17.89	0.43
	Bit 2	20.63	18.36	16.78	17.86	
64QAM	Bit 1	16.62	19.76	25.14	21.07	0.43
	Bit 2	26.23	25.39	25.49	25.34	
	Bit 3	31.12	26.45	23.02	25.32	

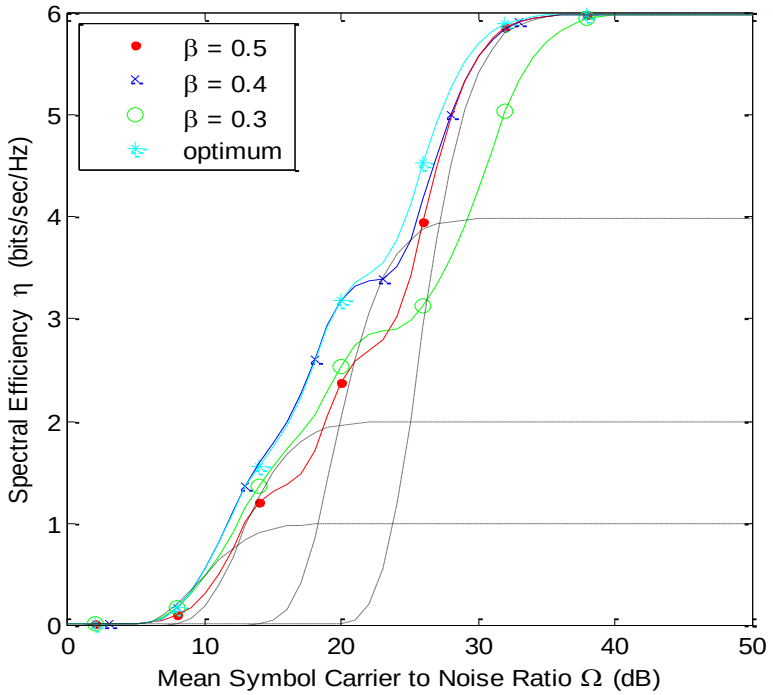

Figure 26: Spectral Efficiency for Different β Values Using QoS 10^{-5} and 10^{-3} (m=3)

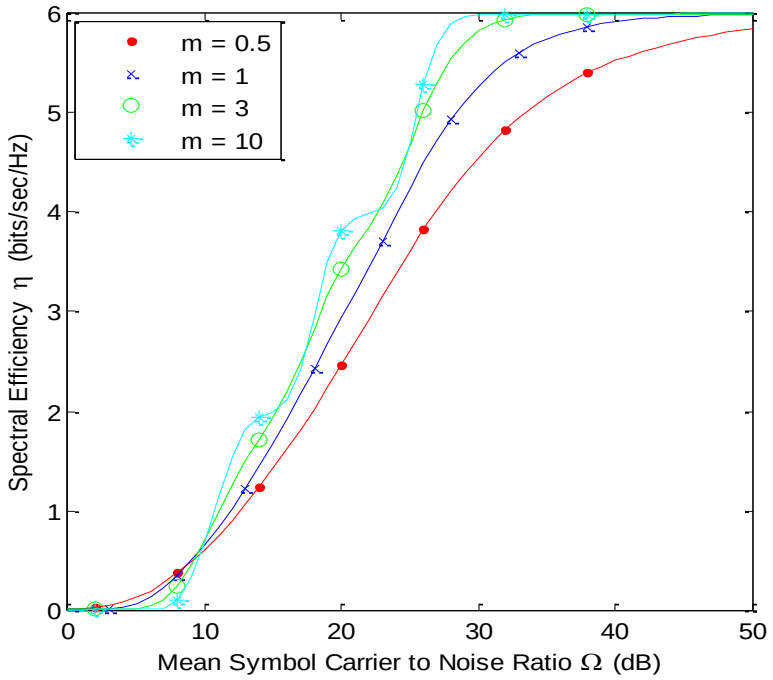

Figure 27: Spectral Efficiency for Different Nakagami-m Fading Parameter Optimum β

For quality of service (QoS) of 10^{-5}, 10^{-4}, 10^{-3} the spectral efficiency can also be found in the similar manner as shown above for the quality of service QoS 10^{-5} and 10^{-3}. The threshold values for the intra-modulation and inter-modulation are listed in Table 22 and 23, respectively. The spectral efficiency of the system in a Nakagami-m fading channel with m = 3 is shown in Figure 27. Again, the result shows different β values including normal transmission in which β = 0.5 and the optimum β value. For this QoS, the optimum beta value has the highest spectral efficiency as compared to the conventional scheme.

Table 22. Threshold Values for Intra-modulation Schemes (dB):QoS 10^{-5}, 10^{-4}, 10^{-3}

Modulation	Bit Class	α, β=0.3	α, β=0.4	α, β=0.5	α, β=optimum	Optimum value
4PSK	Bit 1	13.07	14.91	17.01	14.91	0.4
	Bit 2	19.53	17.57	16.15	17.60	
16QAM	Bit 1	15.72	17.33	19.24	17.90	0.43
	Bit 2	22.07	19.86	18.25	19.36	
64QAM	Bit 1	16.60	19.76	25.18	23.15	0.47
	Bit 2	24.66	24.17	23.97	24.11	
	Bit 3	32.69	29.09	21.86	25.06	

Table 23. Threshold Values for Inter-modulation Schemes(dB):QoS $\frac{10^{-5}+10^{-4}+10^{-3}}{3}$

	4PSK	16QAM	64QAM
$\alpha=\beta$=0.3	15.19	22.17	32.67
$\alpha=\beta$=0.4	12.99	19.95	26.51
$\alpha=\beta$=0.5	11.65	18.53	23.47
$\alpha=\beta$,optimum	12.51	19.44	23.97

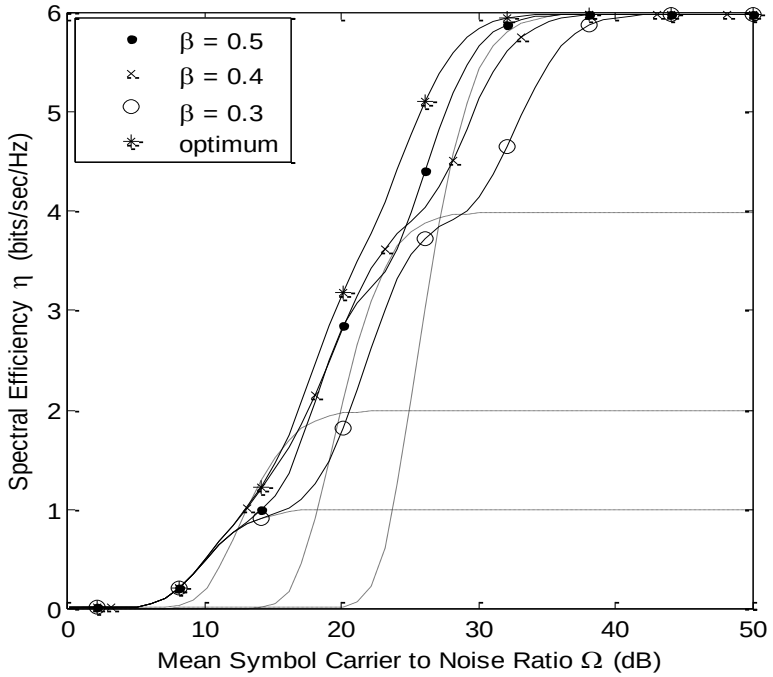

Figure 28: Spectral Efficiency for Different β Values Using QoS 10^{-5} ,10^{-4} and 10^{-3} (m=3)

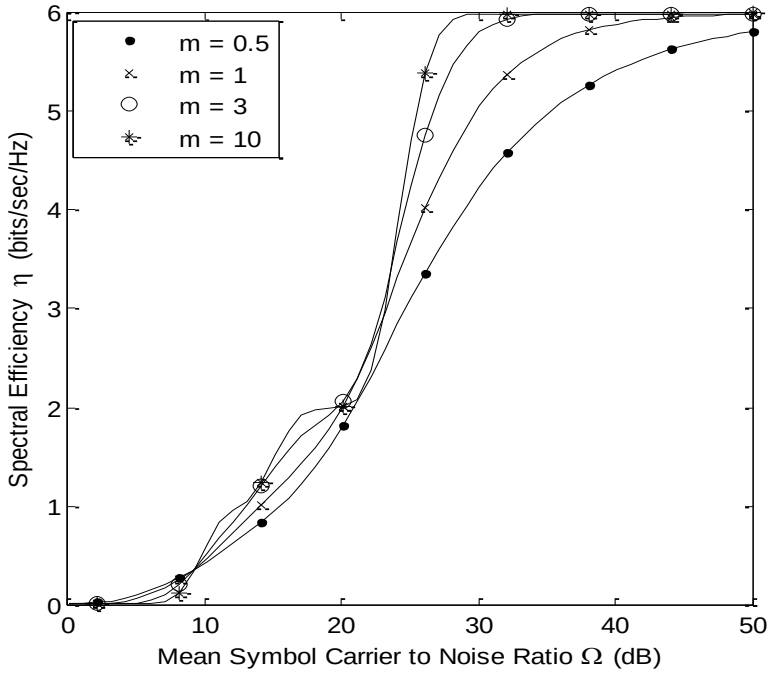

Figure 29: Spectral Efficiency for Different Nakagami-m Fading Parameter, Optimum β

The results from both spectral efficiency plots (i.e. Figure 26 and 28) illustrates that the optimum value of the phase offset ratio are more efficient than conventional scheme and hence this scheme utilizes the available bandwidth more efficiently. Figure 27 and 29 illustrates the spectral efficiency plot for optimum beta value under different Nakagami-m channel conditions. In both Figures 27 and 29, the spectral efficiency is higher for m= 10. This result demonstrates that adaptive multi-resolution modulation has a higher spectral efficiency than conventional scheme, and this is achieved by adapting both the shape and the size of the asymmetric signal constellation. Adaptive multi-resolution modulation improves the throughput for multimedia data while satisfying the distinct QoS requirements for each traffic type under different channel condition.

5.0 UNEQUAL ERROR PROTECTION OF H.264/AVC VIDEO

Novel and robust transmission schemes for video data have to be developed due to the increasing demand for multimedia services over wireless channels. Lately there has been a major focus on the H.264/AVC standard since it offers the best compression efficiency over its predecessors such as MPEG-4 [21] and makes efficient use of the available channel bandwidth. Different types of error resiliency schemes are used in the H.264 video compression standard to reduce the effect of transmission errors. Examples of such schemes in H.264/AVC video coding standard [22, 23] include data partitioning, layered coding, reference frame selection, Flexible Macroblock Ordering (FMO).

In order to minimize the effects of transmission errors on the reconstructed video image quality, Unequal Error Protection (UEP) schemes can be used [24-27]. UEP is based on the idea that more important video data can be given higher protection at the cost of less important data. For example, the picture header and motion vectors are much more important than the texture data. The reconstructed video quality will be severely degraded when errors occur on the important bits. Thus, these important bits should have a higher protection order than the rest of the video bit-stream. Different ways for providing unequal error protection will be discussed shortly.

At the application layer, in order to exploit unequal error protection of the video bitstream, priority partitioning can be used. Here, the video bitstream can be partitioned into segments of different priorities according to their relative impact on the video quality. These priority rankings can then be used in an unequal error protection scheme at the physical layer that increases the robustness of the video transmission [26, 27]. At the physical layer, UEP can be achieved by using Forward Error Correction codes (typically with convolutional codes) or hierarchical (asymmetric) modulation where each bit label position has a different level of protection resulting from judiciously chosen signal constellations.

In [9, 15, 16, 28], the hierarchical modulations were investigated for multimedia applications. In [12], Ramachandran *et al.* have designed a digital HDTV broadcast system using scalable discrete cosine transform based source coding and multi-resolution quadrature amplitude modulation (QAM) under a joint source-channel coding framework. In [29], Chang *et al.* have tried to achieve UEP by matching a hierarchical QAM to H.264 AVC on AWGN channels, where important data is matched to more protected bits in a layered codec. A matched UEP scheme using hierarchical modulation was also

proposed for terrestrial video broadcasting in [30]. In [31], Jiang *et al.* describe another matched UEP scheme where they combine Trellis Coded Modulation (TCM) and non-uniform QAM schemes for transmitting H.264/AVC data.

To date, the joint design of RCPC codes and asymmetric modulation has received very little attention. In this chapter, the UEP scheme at the application layer (i.e., multi-level unequal importance of compressed video data) is combined with the physical layer (joint design of unequal rate convolutional codes or RCPCs and asymmetric 8-PSK modulation) to provide graceful degradation of reconstructed video data during short deep fades in a point to point wireless communication system. New multi-layer UEP schemes are designed and implemented. The H.264 video packets with unequal levels of importance are applied to either the equal rate convolutional or RCPC encoders and then mapped onto an unequally protected asymmetric 8-PSK signal constellation where the MSB has a lower probability of being in error than the LSB.

Since the RCPC codes applied to the 3 priorities have different code rates, the queue lengths of the three priorities would be expected to be different and therefore for a particular source data rate, the queue lengths have to be adjusted to correspond to the RCPC code rate arrangements. This adjustment is crucial as, otherwise, the length of each priority after RCPC encoding would not be the same and it would not be possible to map each bit from every priority in the MSB-to-LSB fashion onto the asymmetric 8PSK constellation.

5.1. H.264/AVC Video Standard and Prioritization

The H.264/AVC video coding standard [32-34], proposed by the Joint Video Team (JVT) of ITU-T and ISO/IEC, achieves a significant improvement in the compression efficiency over the other existing standards. This makes H.264 AVC a favorable candidate for all future multimedia applications.

The H.264/AVC standard is composed of two layers namely the Video Coding Layer (VCL) for video compression and Network Abstraction Layer (NAL) for transport of compressed video data over networks [32]. NAL works in two kinds of mode: Single Slice mode and Data Partition mode. When using Data Partition mode, H.264 puts all variable length codes with the same data type together in each frame.

Head information includes head information, macroblock type, frame type, predicted residual of motion vectors, frame flag and this part is called Data Partition A (DP A), which is the most important part. Intra-frame segmentation is called Data Partition (DP B). It loads the coding mode and the

correlation coefficient in intra frame blocks. Compared with information of inter-frame data partitions, intra-frame information can prevent further drift, thus it is more effective than inter-frame data partitions. Inter-frame segmentation is called Data Partition C (DP C). It only includes the coding mode and the correlation coefficient in inter-frame block; it is the biggest segmentation in the video stream. Without receiving the DPA data of a slice correctly, DP B and DP C packets cannot be decoded, thereby discarding the whole slice data. Whereas if a DP C is lost, then the slice can be decoded using the received DP A and DP B information [27, 34].

The output of the H.264/AVC source can be organized in packets of varying importance, depending on the frame type, DP type and slice group. Therefore we can exploit the unequal importance of video data at the application layer by packetizing all the important data together, prioritizing them accordingly and give more protection to them. The H.264/AVC bitstream is split into three priorities, with the Data partitioning mode *'ON'* and the data of each GOP is differentiated based on the frame type and DPs. In order to exploit unequal error protection at the application layer the three priority queues have been designed as follows [27]:

- Priority 1 Queue: IDR frame, DPA of I frame, and DPB of I frame (if queue 1 can accommodate, else move data to queue 2)
- Priority 2 Queue: DPA of P frame, DPA of B frame, and DPC of P frame (if queue 2 can accommodate, else move data to queue 3)
- Priority 3 Queue: DPC of P frame, DPB of B frame, and DPC of B- frame

It should be noted that data packets from the lowest priority queue can be dropped if necessary. This mechanism will help in maintaining equal lengths of the three queues.

5.2. Convolutional Codes and Asymmetric 8PSK Modulation

Information theory tells us that for optimal communications we should design long sequences of signals, with maximum separation among them; and at the receiver we should perform decision making over such long signals rather than individual bits or symbols. If this process is done properly, then the message error probability will decrease exponentially with sequence length, n provided that the rate R is less than R_0, which in turn is less than the Shannon Capacity as given by Equation (34) [35, 36].

$$P_e < Ke^{-(R_0-R)n} \tag{34}$$

Convolutional codes are *channel codes* widely deployed in communication systems to encode digital data before transmission through noisy error-prone channels. For example, convolutional codes

are applied in the GSM system and in deep space and satellite communications for encoding of information bits. A *(n,k,m)* convolutional encoder is one that maps *k* input bits to *n* output bits giving rise to a code rate of *k/n* coded bitstream. *m* is the number of shift registers in the encoder. The *n* encoder outputs at a given time unit depends not only on the *k* input bits at that time but also on the *m* previous input bits. At the receiver, the transmitted bitstream can be decoded to recover the original data, correcting errors in the process. The Viterbi Algorithm [37, 38] is the most popular algorithm for maximum-likelihood decoding due to its lower complexity implementation as compared to other algorithms e.g. sequential decoding. The possible received bit sequences form a trellis structure and the Viterbi algorithm tracks likely paths through the trellis before choosing the most likely path.

RCPC codes achieve UEP by puncturing off different amounts of coded bits of the parent code [38, 39]. The ordinary convolutional code to be punctured is called the parent code and the resulting RCPC codes are called the children codes. Compared with the parent code, RCPC codes are of higher rates and give poorer BER performance but RCPC codes can easily provide flexible choices of code rates. Many applications of RCPC codes have been proposed in recent years [40-42].

5.2.1. Theoretical Bit Error Rate Analysis

To calculate theoretical bounds for the Bit Error Rate P_b of a convolutional code we can use the estimate based on unquantized-decision decoding given by Equation (35) [37, 38]. In this estimate, c_d is the sum of bit errors for error events of distance *d*, and *f* is the free distance of the code. The quantity P_d is the pair wise error probability that the wrong path at distance $\boldsymbol{d}$ is selected. Values for the coefficients c_d and the free distance *f* are obtained in published articles such as [38, 39].

$$P_b \leq \sum_{d=f}^{\infty} C_d P_d \qquad (35)$$

Let *x* be the signal being transmitted after convolutional encoding and ρ is the real Rayleigh distributed random variable with $E(\rho^2)=1$ and *n* is the complex one-sided Power Spectral Density (PSD) of Additive White Gaussian Noise (AWGN). Then the corrupted signal can be expressed as

$$y = \rho.x + n \qquad (36)$$

In this way *x* encounters random amplitude and phase variations as well as white Gaussian noise over the wireless channel. In this work it is assumed that the coherent receiver operates without the knowledge of Channel State Information (CSI). As explained by Hagenauer and Viterbi [37, 38] the

performance of convolutional codes using hard-decision decoding over Gaussian and Rayleigh channels in terms of P_d is given by

$$P_d = \begin{Bmatrix} \sum_{e=d+1/2}^{d} \binom{d}{e} P_0^{\,e}(1-P_0)^{d-e} \text{ for } d \quad odd \\ \frac{1}{2}\binom{d}{d/2} P_0^{\,d/2}(1-P_0)^{d/2} + \sum_{e=\frac{d}{2}+1}^{d} \binom{d}{e} P_0^{\,e}(1-P_0)^{d-e} \text{ for } \quad d \quad even \end{Bmatrix} \quad (37)$$

where P_0 is the channel bit error rate given by

$$P_0 = \frac{1}{2} erfc\left(\frac{E_b}{N_0}\right) \text{ assuming } E(\rho^2)=1 \quad (38)$$

P_d can be used in the theoretical evaluation of the Bit Error Rate P_b given by Equation (35). Lin *et al.* [36] proved mathematically that since P_0 is small, P_b can be directly computed from a knowledge of P_0 and d_{free}. This theoretical upper bound is given in [36] as:

$$P_b = \frac{1}{k} C_{dfree} 2^{dfree} P_0^{\,dfree/2} \quad (39)$$

where C_{dfree} refers to the information error weight at distance $d=d_{free}$ and k is the number of information bits of the mother code. These parameters can be obtained from Hagenauer [38].

5.2.2. Asymmetric 8PSK Modulation

The general model of multi-resolution signaling (also known as embedded or non-uniform constellation model) can be found in [19]. In this work, the non-uniform 8-PSK constellation, with $m = log_2 8 = 3$ hierarchical levels is considered. Consider a non-uniform 8-PSK constellation depicted in Fig. 30. The actual symbols are represented by small circles and are Gray coded. The first level and the second level virtual signal points are represented by "*x*" and "+" respectively. The phase offset angles for general non-uniform PSK constellation θ_i are simplified as follows[17, 27]:

$$\theta_i = \frac{\pi}{2}\beta^i, i = 1,2,\ldots,m-1$$

where $m = \log_2 M$ where M is the alphabet size. The reason for fixing the ratio of the angles for any subsequent levels of the signal constellation hierarchy β to a constant is to facilitate the phase offset

optimization (i.e., only a single parameter needs to be optimized rather than manipulating (*m*-1) variables [17]).

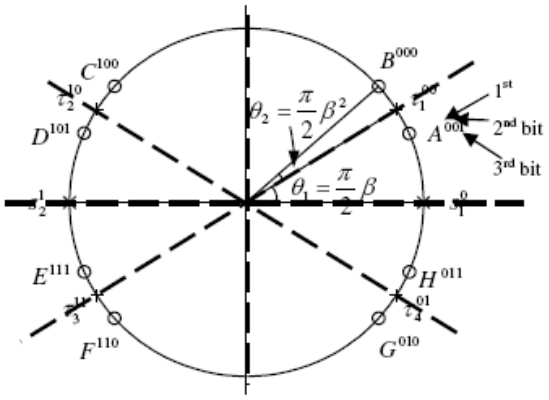

Figure 30: Asymmetric 8 PSK Constellation [19, 27]

Furthermore, when the phase offset ratio β = 0.5, the system reverts to a uniform 8-PSK constellation. It has been shown, through simulation results, that the modulator achieves highest degree of Unequal Error Protection among the three levels when beta ranges from 0.4 to 0.5 [27]. Therefore, in this research work all simulations carried out take the range of values of β between 0.4 and 0.5. Also, the modulator is designed and implemented based on the following mapping rules [27]:

Phase Angle	***Signal***	***Symbol***
$(\beta*\pi/2) + (\pi/2*\beta^2)$	S_0	*000*
$(\beta*\pi/2) - (\pi/2*\beta^2)$	S_1	*001*
$(2*\pi) - ((\beta*\pi/2)+(\pi/2*\beta^2))$	S_2	*010*
$(2*\pi) - ((\beta*\pi/2)-(\pi/2*\beta^2))$	S_3	*011*
$\pi - ((\beta*\pi/2)+(\pi/2*\beta^2))$	S_4	*100*
$\pi - ((\beta*\pi/2)-(\pi/2*\beta^2))$	S_5	*101*
$\pi + ((\beta*\pi/2)+(\pi/2*\beta^2))$	S_6	*110*
$\pi + ((\beta*\pi/2)-(\pi/2*\beta^2))$	S_7	*111*

5.3. Method: UEP System Design and Implementation

The design and implementation of the proposed Multi-layer UEP scheme employing prioritized H.264/AVC video data at the application layer and convolutional codes as well as RCPC codes with asymmetric 8-PSK modulation at the physical layer are explained in detail in this section.

5.3.1. Multi-layer UEP Scheme Using Equal Code Rate Convolutional Codes and Asymmetric 8PSK Modulation

Unequal error protection is achieved at the physical layer by using equal code rate convolutional codes and asymmetric 8PSK modulation. Fig. 31 shows the complete design process in the form of a block diagram. In order to create an unequal error protection scheme at the physical layer, we applied equal rate convolutional code to each queue coming from the prioritized H.264 video output. The outputs of the three convolutional codes after encoding are then multiplexed to form an asymmetric 8PSK symbol. For example, consider the H.264 video outputting a bit rate of 512 kbps, then the length of each queue would be $r_1=r_2=r_3=$ 512kbps/3 and by applying a ½ -rate convolutional code to every queue that is, $R_1=R_2=R_3=$ ½ , the output data rate would be 1024 kbps. In this way, we obtained a physical layer design with an overall rate of ½.

The asymmetric modulated symbol is sent over the wireless channel and the received bit stream is demodulated using Asymmetric 8-PSK demodulation. The bitstream is then demultiplexed and fed to the corresponding Viterbi decoder and the queues are arranged in order of their priorities and inputted to the H.264 decoder. As H.264/AVC is not designed to handle bit errors, any bit errors will lead to discarding of the packet. The bitstream with packet drops is given to the robust H.264/AVC decoder which reconstructs the video frames with the help of error concealment techniques.

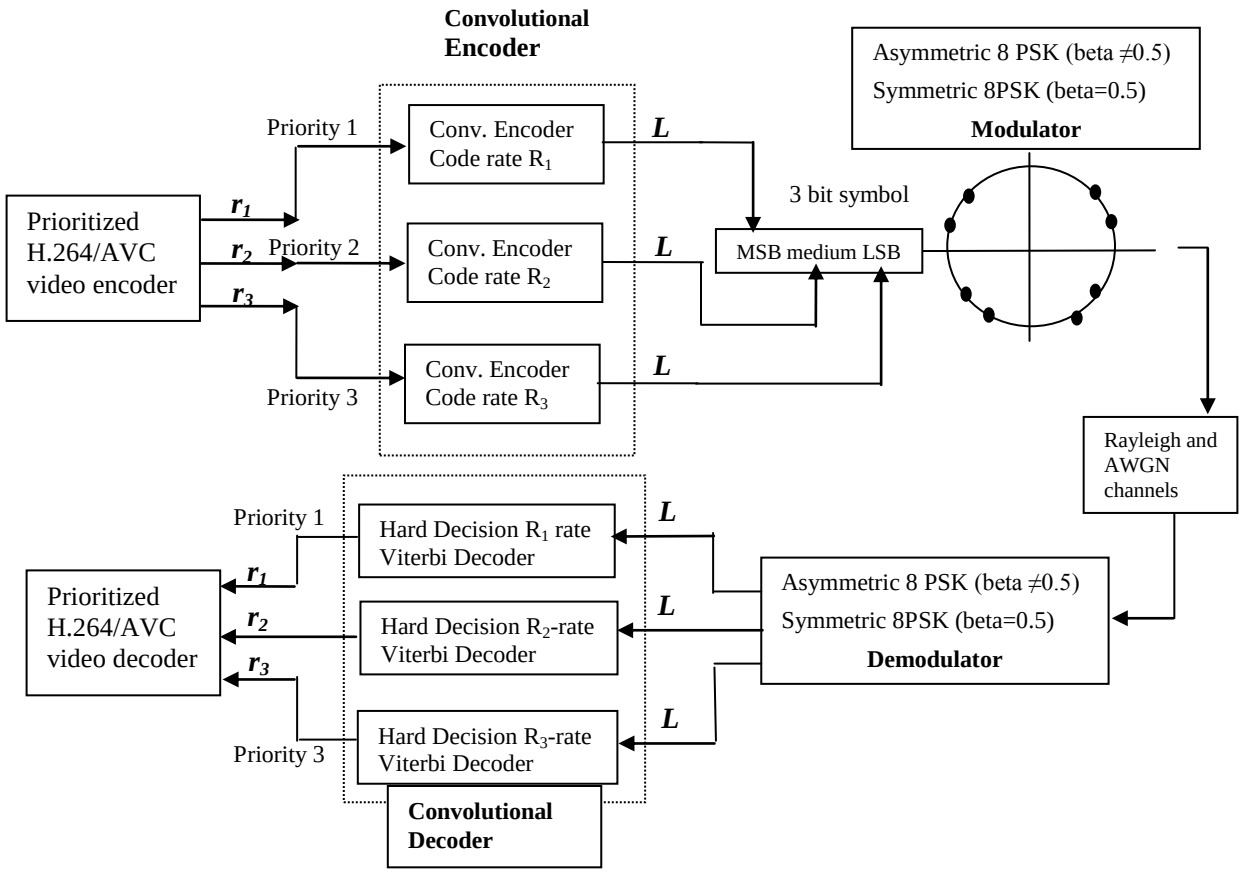

Figure 31: Block diagram of designated multi-layer UEP scheme using equal code rate convolutional codes

Table 24 lists the different H.264 source video bitrates as well as the convolutional code rates used and the gross output channel data rate. In all the cases, a mother code rate ½ with puncturing periods of 8 and 6 has been used to generate convolutional code rates of 2/3, 3/4 and 4/5 as suggested by Hagenauer [38] and Lee [39]. The puncturing matrices are also given in Table 24 and in all cases the generator polynomials was 23 and 35 (octal format) with constraint length K=5.

Table 24. H.264 video bitrates, convolutional code parameters and output channel data rates

	Total H.264 Video bitrates	Convolutional code on each priority G = [23 35] and K=5, Puncturing matrix and period Hagenauer [38] and Lee [39]			Total channel data rate
(a)	512 kbps	1/2	1111 1111 1111 1111	8	1024 kbps
(b)	683 kbps	2/3	1111 1111 1010 1010	8	1024 kbps
(c)	768 kbps	3/4	111 111 100 100	6	1024 kbps
(d)	820 kbps	4/5	1111 1111 1000 1000	8	1024 kbps

5.3.2. Multi-layer UEP Scheme Using RCPC Codes and Asymmetric 8PSK Modulation

At the physical layer three RCPC codes, given by Hagenauer [38], are appropriately chosen so that a desired overall rate of either ½, 2/3, ¾ or 4/5 is obtained and these RCPCs are applied to the 3 priorities. The same design of Fig. 31 is used except that here code rates R_1, R_2 and R_3 are unequal resulting in unequal video source rates r_1, r_2 and r_3. To achieve an overall rate of ½, the three RCPCs chosen are 8/18, 8/16 and 8/14 with puncturing period of 8, constraint length K=5 and generator polynomials 23, 35 in octal format. Table 25 gives the RCPC code parameters used in the design.

Table 25. RCPC code parameters for overall ½-rate UEP scheme

RCPC codes Constraint length K=5, Table 24 Hagenaeur [38]			
Priority	**Coderate**	**Punctured vector**	**Generator polynomials**
1	8/18	[11111111 11111111 10001000]	23,35,27
2	8/16	[11111111 11111111]	23,35
3	8/14	[11111111 11101110]	23,35

From the design of Fig. 31, if the total source data rate is denoted as R, then according to the RCPC coderate arrangements, the percentage of data that should be fed to each priority can be found by using simple proportions as follows:

$$r_1 = \frac{R_1}{R_1 + R_2 + R_3} \times R \quad \text{or} \quad r_1 = \frac{\frac{8}{18}}{\frac{8}{18} + \frac{8}{16} + \frac{8}{14}} \times R = 0.29R \tag{40}$$

$$r_2 = \frac{\frac{8}{16}}{\frac{8}{18} + \frac{8}{16} + \frac{8}{14}} \times R = 0.33R \tag{41}$$

$$r_3 = \frac{\frac{8}{14}}{\frac{8}{18} + \frac{8}{16} + \frac{8}{14}} \times R = 0.38R \tag{42}$$

In this chapter, we use the H.264/AVC standard with a source bitrate of 512 kbps. Hence the value of R is equal to 512 kbps in Equations (40) to (42). The queue lengths of priority 1, 2 and 3 can be obtained from Equations (40) to (42) and equal to 29%, 33% and 38% respectively. The H.264/AVC

prioritized source video outputs data at a bitrate of 512kbps and since unequal code rate convolutional codes are used then the queue length of each priority are divided in 29%, 33% and 38% proportions. The total channel data rate would be 1024 kbps.

Other overall 2/3, 3/4 and 4/5-rate multi-layer UEP schemes are designed and implemented in a similar way as explained above except that for a particular overall rate UEP scheme the RCPC code arrangements and source bitrate are varied so that the total channel data rate is maintained at 1Mbps and hence a fair comparison can be done among the designed UEP schemes. Table 26 gives the physical layer parameters used in the design of various overall rate multi-layer UEP schemes. Different source bitrates are used and the amount of data in each queue, calculated from Equations (40) to (42), varies according to the RCPC code arrangements.

Table 26. Physical layer parameters for overall rates of 2/3, 3/4 and 4/5 UEP schemes

Overall rate multi-layer UEP schemes	**RCPC codes Constraint length K=5, Generator Polynomials =23, 35. Table 24 Hagenaeur [38]**			**% proportions**	**Total H.264/AVC source bitrate**	**Total Channel data rate**
	Priority	**Coderate**	**Punctured vector**			
2/3	1	8/14	[11111111 11101110]	28	683 kbps	1024 kbps
	2	8/12	[11111111 10101010]	33		
	3	8/10	[11111111 10001000]	39		
¾	1	8/14	[11111111 11101110]	26	768 kbps	1024 kbps
	2	8/10	[11111111 10001000]	37		
	3	8/10	[11111111 10001000]	37		
4/5	1	8/12	[11111111 10101010]	27	820 kbps	1024 kbps
	2	8/10	[11111111 10001000]	32		
	3	8/8	-	41		

5.4. Results and Discussion

The experiments were set up by using the H.264/AVC Annex B (JM14.1) reference source code [32, 33] for encoding the CIF (352x288 pixels) Bus video test sequence at the various bit rates mentioned in earlier sections. The video sequence was encoded at 30 frames/second for a GOP of 12 frames (IDR B P B P B P B P B P B I ...) with an IDR rate of 24 frames. The following error resiliency features were enabled: data partitioning, FMO dispersed mode and Constrained Intra Prediction. The NAL size of 200 bytes was considered and a robust decoder with error concealment schemes was used.

Two channel models namely Rayleigh and AWGN have been used in the simulations. The built in MATLAB R2008a Simulink AWGN and Rayleigh channel models, from the communications block set, were used. The experiments were conducted by varying the CNR from 10dB to 28dB in steps of 2 dB and by varying asymmetric 8-PSK modulation design parameter β from 0.42 to 0.50 in steps of 0.02. Each experiment was repeated 10 times with different random seeds and the obtained results were averaged. For our simulations, we used Visual Studio 2005 to compile the H.264/AVC source code, MATLAB R2008a Simulink to simulate the physical layer and Cygwin to automate the complete system.

Fig. 32 presents the PSNR curves against the variation of beta for overall code rates of 2/3, 3/4 and 4/5 at different CNR values. It can be seen that for CNR values of 16, 18 and 20 dB asymmetric 8PSK (β <0.5) and RCPC codes perform better than the symmetric case at β =0.5. Furthermore, the improvement with β <0.5 increases as the code rate is increased. At low CNRs, asymmetric modulation compensates for the weak (high rate) code.

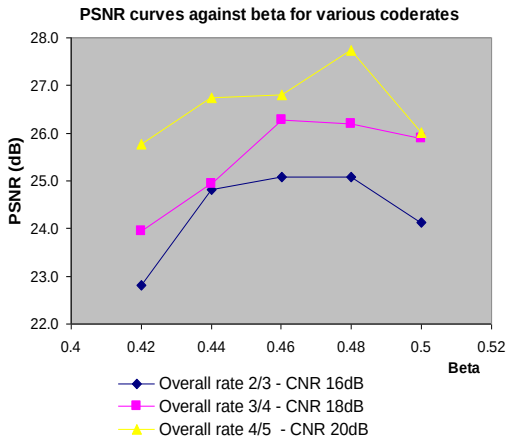

Figure 32: PSNR curves against beta for overall code rates employing RCPC codes

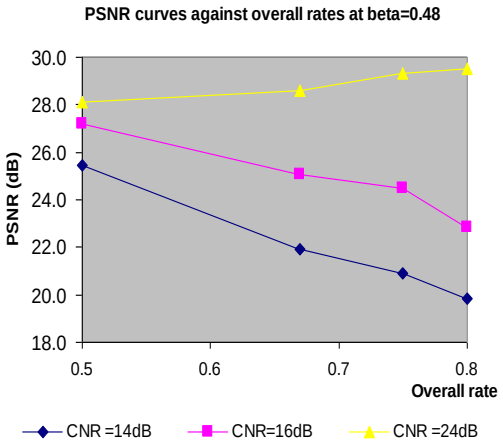

Figure 33: PSNR curves against overall rates at beta=0.48

PSNR curves are plotted against the overall code rates at β =0.48 and shown in Fig. 33. It can be observed that at low CNR values of 14 and 16 dB, the PSNR values decrease with increasing overall rates. This is explained by the fact that as overall rates increase at a low CNR, the UEP scheme becomes less powerful with the use of weak RCPC codes. However, at a high CNR value of 24 dB, the PSNR values increase with increasing overall rates which indicates that the UEP schemes tend to achieve error-

free PSNR values. Table 27 lists the error-free PSNR values for the BUS CIF sequence with NAL of 200 bytes at various source video bit rates.

Table 27. Error-free PSNR values for Bus CIF sequence, NAL 200 bytes

Source bit rate	**Average code rate**	**PSNR value (dB)**
512 kbps	½	28.1524
683 kbps	2/3	28.9253
768 kbps	¾	29.7167
820 kbps	4/5	30.1365
1024 kbps	1 (uncoded)	31.5680

Fig. 34 shows the performance curves, at β =0.48 for various code rates employing equal rate convolutional codes as well as for the uncoded case, which is without the use of FECs. It can be clearly seen that the overall rate ½ code gives significant coding gain of around 7 dB over uncoded asymmetric modulation at a CNR of 18 dB. The coding gains for the overall rates of 2/3 and ¾ are approximately 5 and 3 dB respectively at the same value of CNR. This reduction in coding gain can be explained by the fact that as the convolutional code rate is increased, the UEP scheme becomes less powerful over the chosen low CNR range. As the CNR increases, higher rate codes can be used. As can be seen from Fig. 34, the gap narrows at the CNR of 28 dB and higher rate codes will be better at the higher CNR values.

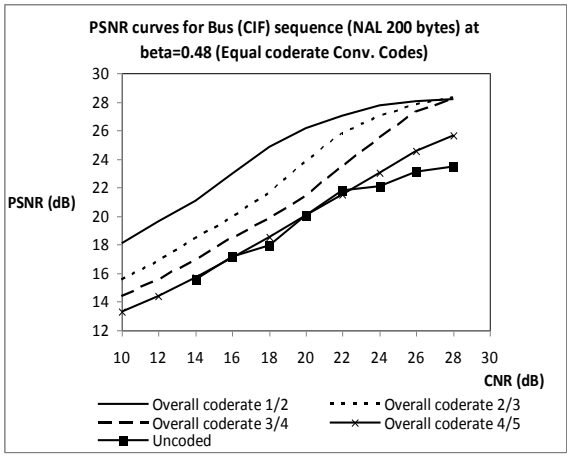

Figure 34: PSNR curves for various code rates and uncoded asymmetric 8PSK modulation at beta=0.48

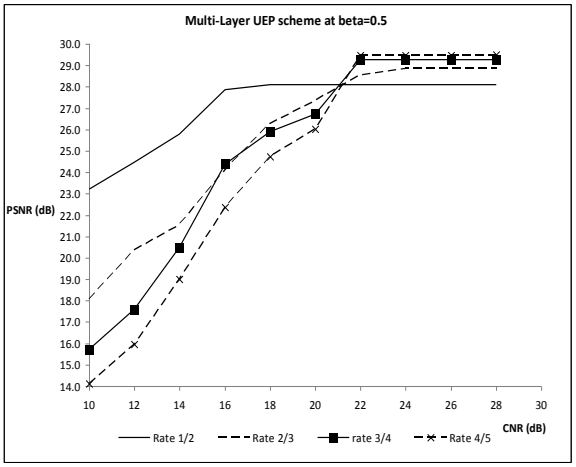

Figure 35: Performance curves for multi-layer UEP scheme at beta=0.5

In Fig. 35 the performance of the multi-layer UEP scheme employing various overall rates are plotted against the CNR at β=0.5. It can be seen again that at low CNR, the performance of the UEP

scheme worsens as the overall rate increases. Once again, as the CNR increases, higher code rates gradually narrow the gap and eventually outperform the overall rate ½ code. At high CNR values, all UEP schemes approach the error-free PSNR corresponding to the overall rate of the system. At a CNR value of 18 dB, the multi-layer UEP scheme based on overall ½-rate gives coding gains of approximately 2.5 and 3.5 dB over the corresponding 3/4 and 4/5 rates, respectively.

The performances of various multi-layer UEP schemes employing equal-code rate convolutional codes as well as RCPC codes are compared and shown in Figs. 36 and 37 for overall rates of ½, 2/3, ¾ and 4/5 at β=0.48. The UEP scheme based on ½-rate RCPC codes outperforms the one employing equal ½-rate convolutional code by approximately 3 dB in PSNR improvement at a CNR of 18dB. This improvement is due to the fact that the RCPC codes can give further selective protection to the high priority packets (beyond that given by the asymmetric modulation). Since the equal ½-rate convolutional code UEP scheme yields a coding gain of 7 dB over the uncoded asymmetric modulation at the same CNR and β values as shown in Fig. 34, this ½-rate RCPC UEP scheme would give a significant coding gain of (3+7) =10 dB gain in PSNR over uncoded asymmetric modulation. Around a 4 dB coding gain can be observed for the UEP schemes based on overall rate of 2/3 at this same value of CNR of 18dB.

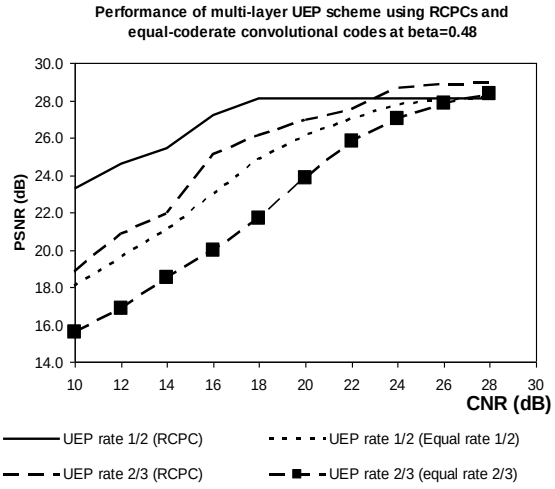

Figure 36: Performance curves for multi-layer and 1/2 and 2/3 overall rate UEP schemes

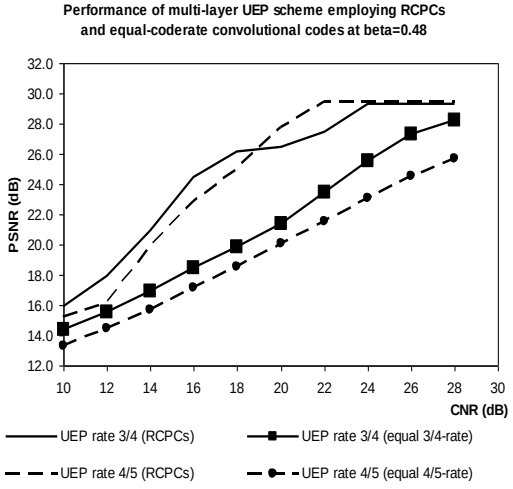

Figure 37: Performance curves for multi-layer 3/4 and 4/5 overall rate UEP schemes

Figs. 38 - 40 show the test video frames with the various multi-layer UEP schemes that have been designed and implemented in this work. It can be clearly observed that all UEP schemes employing unequal rate (RCPC) codes outperform the corresponding equal rate convolutional codes. The frame numbers at which the best performance occurs for all schemes together with the PSNR, CNR as well as β values used in the simulations are shown.

Frame No. 41

(a) Equal coderate Conv. codes- rate ½ scheme
PSNR 23 dB, CNR 18dB, beta=0.5, Frame Nos. 20-42

Frame No. 41

(b) RCPC– rate ½ scheme
PSNR 28 dB, CNR 18dB, beta=0.5, Frame Nos. 20-42

Figure 38: Test video pictures for multi-layer overall rate 1/2 schemes

Frame No. 27

(a) Equal coderate Conv. codes- rate 2/3 scheme
PSNR 18 dB, CNR 14dB, beta=0.5, Frame Nos. 24-47

Frame No. 27

(b) RCPC– rate 2/3 scheme
PSNR 21 dB, CNR 14dB, beta=0.5, Frame Nos. 24-47

Figure 39: Test video pictures for multi-layer overall rate 2/3 schemes

Frame No. 88

(a) Equal coderate Conv. codes- rate ¾ scheme
PSNR 19 dB, CNR 16dB, beta=0.5, Frame Nos. 84-107

Frame No. 88

(b) RCPC– rate 3/4scheme
PSNR 22 dB, CNR 16dB, beta=0.5, Frame Nos. 84-107

Figure 40: Test video pictures for multi-layer overall rate 3/4 schemes.

5.4.1. Bit Error Rate Analysis for UEP Schemes Employing RCPC Codes

As explained earlier in Section 5.2.1, the theoretical bound for the BER, P_b, of a convolutional code is given by Equation (39). We can use this formulation to compute the theoretical BER of our proposed multi-layer UEP schemes employing RCPC codes. Table 28 gives the parameters used to compute the theoretical P_b of the highest priority packets for all multi-layer UEP schemes designed in this chapter.

Table 28. Code parameters of priority 1(Highest) for all multi-layer RCPC UEP schemes

Overall rate multi-layer UEP scheme	Priority 1 (Highest) convolutional code rate. Hagenauer [38]	C_{dfree}	d_{free}	k
½	8/18	2	5	Mother code (2,1): $k=1$
2/3	8/14	2	4	
3/4	8/14	2	4	
4/5	8/12	4	3	

Fig. 41 presents the simulated bit error rate performances for all multi-layer RCPC UEP schemes designed and implemented in this chapter. Also, the theoretical bounds are plotted for each UEP scheme based on the parameters given in Table 28. It can be seen that the theoretical and simulated results closely agree for all the UEP schemes.

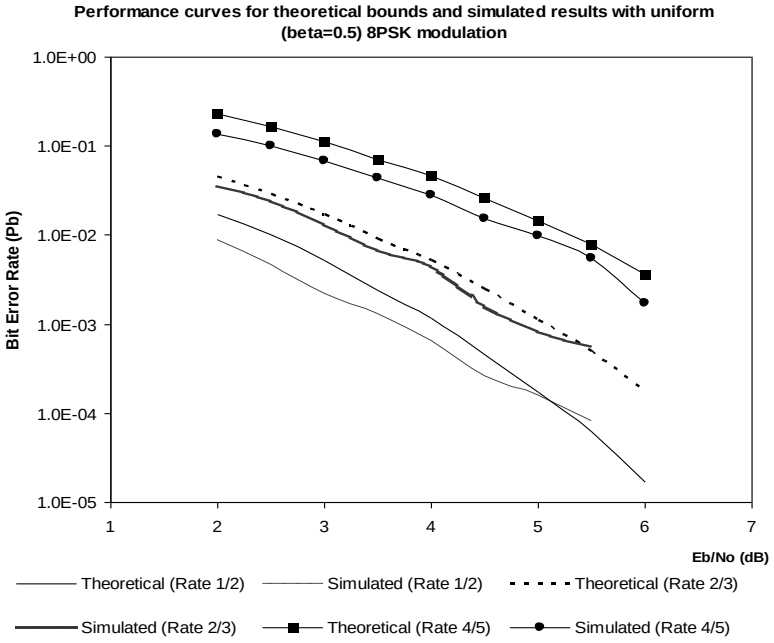

Figure 41: Theoretical and simulated bit error performances for various multi-layer RCPC UEP schemes with symmetric 8PSK modulation (β=0.5).

In Fig. 42 the simulated bit error rate performances for overall rates of 1/2, 2/3 and 4/5 are plotted for the symmetric case at β=0.5 and asymmetric case at β=0.48. It can be clearly seen that all asymmetric results outperform the corresponding symmetric cases. This clearly validates the joint use of RCPC codes and asymmetric modulation in a UEP scheme. The performance of each of the three priorities is better with the joint design, thus resulting in significantly higher video PSNR. Furthermore, the results are consistent over a wide range of CNRs, suggesting that the proposed scheme is suitable for use in a wireless system where the CNR fluctuates due to fading. At a Bit Error Rate of 10^{-4}, the ½-rate UEP scheme employing RCPC codes and asymmetric 8PSK modulation with β=0.48 gives about 1.5 dB gain over its symmetric counterpart.

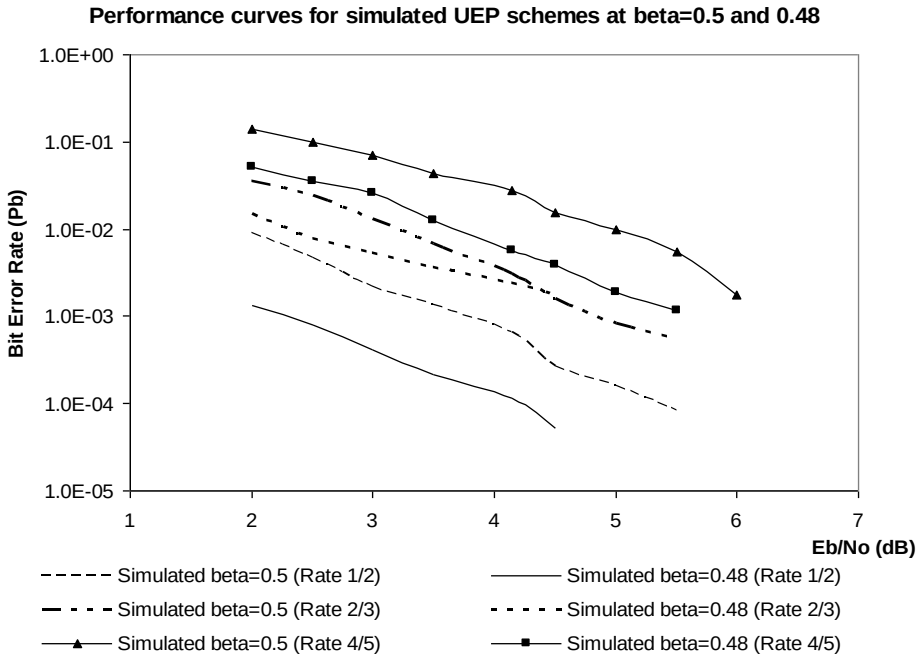

Figure 42: Simulated bit error performances for various multi-layer RCPC UEP schemes with 8PSK modulation (symmetric and asymmetric cases)

6.0 CONCLUSIONS AND FUTURE RESEARCH DIRECTIONS

6.1 Conclusions

The primary problem in adaptive modulation is to find a simple way to effectively match the "shape" of hierarchical modulation at the physical layer to the bit streams given different QoS requirements at the application layer. The exact closed-form expressions for the BER are hard to find for non-binary modulation techniques. The exact closed-form expressions are not easily inverted or easily differentiated with respect to their arguments. In this report, closed-form expression for the BER using the complementary error function was developed. The complementary error function BER approximation expression is compared to previously-used exponential function BER approximation. The comparison revealed that complementary error function BER approximation gives better result than previously-used exponential function BER approximation.

Earlier work done by Hayes [4], Covers [5], Hentinen [6] and Annamalai et al [7, 8] on link adaptation showed that, in a time-varying wireless network, the spectral efficiency can be improved dynamically by link adaptation techniques. However, the classical transmitter-oriented rate adaptation method proposed suffers from a number of limitations. This research addressed these limitations by taking into account the fixed signal constellation size and the limitations. The limitations are counteracted by designing adaptive hierarchical modulation for supporting multimedia traffic over generalized multipath fading channels. The major difference is that unlike previous adaptive technique which only considered homogenous traffic, our adaptive technique is designed for heterogeneous traffic.

Challenges such as limited battery life and fluctuation of the wireless link are some of the problems faced by wireless systems for supporting multimedia traffic. In this report, an adaptive multi-resolution modulation was proposed for supporting multimedia traffic. This scheme improves the

throughput for all the multimedia data, while satisfying the distinct quality of service (QoS) requirements for each traffic type under different channel condition. This is done by adapting the size of digital signal constellation based on the prevailing channel conditions, with an objective of improving the spectrum utilization efficiency without wasting power or sacrifice BER performance. The battery life is improved by adapting both the shape and the size of the asymmetric signal constellation.

6.2 Contributions

Bit error rate approximation for hierarchical quadrature amplitude modulation (QAM) was developed in terms of complementary error functions. The complementary error functions BER approximation produces better curve fitting result as compare to exponential function BER approximation. Hence the erfc approximation produces better result in finding the required thresholds for different modulation scheme in adaptive modulation.

The efficacy of a receiver-oriented rate-adaptation scheme using hierarchical QAM for sustaining the quality of randomly fluctuating wireless links in mobile ad-hoc networks at a desired level was investigated. This scheme allows for graceful signaling rate reduction in wireless ad-hoc networks when the channel condition deteriorates for a short period of time.

The effectiveness of adaptive multi-resolution modulation for multimedia transmission (including H.264 compressed video) over flat fading channels was considered. In this case, an adaptive hierarchical modulation signaling technique is designed to take advantage of the differences in the QoS requirements among different bit streams at the application layer.

6.3 Future Research and Recommendations

In this research, we assumed that the channel condition is always desirable for the proposed adaptive modulation schemes and therefore retransmission was not taken into consideration. A joint-design of multi-resolution modulation with retransmission diversity for integrated real time/delay-

tolerant services which takes into account the disparity in QoS requirements for different message types as well as the packet loss due to queuing is to be investigated.

7.0 REFERENCES

1. Seong Taek Chung and A. Goldsmith, "Degrees of Freedom in Adaptive Modulation: A Unified View," *IEEE Trans. Communications*, Volume.49, no.9, pp.1561-1571, Sep 2001.
2. Annamalai, A., Jing Lu, Vaman, D.R., "A Receiver-Oriented Rate-Adaptation Strategy for Improving Network Efficiency in Mobile Ad-Hoc Networks," *IEEE Sarnoff Symposium*, pp.1-5, 28-30 April 2008.
3. Annamalai, A., Vaman, D., Matyjas, J. and Medley, M., "Joint-Design of Multi-Resolution Modulation and ARQ Protocol for Prioritized Packet Transmission in Wireless Ad-Hoc Networks," *IEEE Military Communications Conference*, pp.1-7, 16-19 November 2008.
4. J. F. Hayes, "Adaptive Feedback Communications," *IEEE Trans. Communications Technology*, Volume 16, pp. 29-34, February 1968.
5. J. Cavers, "Variable-rate Transmission for Rayleigh Fading Channels," *IEEE Trans. Communications*, pp. 15-22, Volume 20, February 1972.
6. V. Hentinen, "Error Performance for Adaptive Transmission on Fading Channels," *IEEE Trans. Communications*, Volume 22, pp. 1331-1337, September 1974.
7. A. Annamalai and V. K. Bhargava, "Simple and Efficient Techniques to Implement a Self-Reconfigurable ARQ System in a Slowly Varying Mobile Radio Environment," *International Journal on Wireless Personal Communications:* Volume 13, pp. 97-117, May 2000.
8. A. Annamalai and V. K. Bhargava, "Analysis and Optimization of Adaptive Multicopy Transmission ARQ Protocols for Time-Varying Channels," *IEEE Trans. Communications*, Volume 46, No. 10, pp. 1356-1368, October 1998.

9. M. Pursley and J. Shea, “Adaptive Nonuniform Phase-Shift-Key Modulation for Multimedia Traffic in WirelessNetworks,” *IEEE J. Selected Areas in Communications,* Volume 18, pp. 1394-1407, August 2000.
10. Hossain, Md.J., Vitthaladevuni, P.K., Alouini, M.-S., Bhargava, V.K., Goldsmith, A.J., "Adaptive Hierarchical Modulation for Simultaneous Voice and Multiclass Data Transmission over Fading Channels," *IEEE Trans. Vehicular Technology*, Volume 55, no.4, pp.1181-1194, July 2006.
11. T. Cover, “Broadcast Channels,” *IEEE Trans. Information Theory*, Volume IT-18, pp. 2-14, January 1972.
12. K. Ramchandran, A. Ortega, K. Metin Uz, and M. Vetterli, “Multi-resolution Broadcast for Digital HDTV Using Joint Source/Channel Coding,” *IEEE J. Selected Areas in Communications*, Volume 11, pp. 6-23, January 1993.
13. Y. S. Chan, J. W. Modestino, Q. Qu, and X. Fan, “An End-to-End Embedded Approach for Multicast/Broadcast of Scalable Video over Multiuser CDMA Wireless Networks,” *IEEE Trans. Multimedia*, Volume 9, pp. 655-667, April 2007.
14. M. Sajadieh, F. Kschischang, and A. Leon-Garcia, “Modulation Assisted Unequal Error Protection over Fading Channel,” *IEEE Trans. Vehicular Technology*, Volume 47, pp. 900-908, August 1998.
15. M. Pursley and J. Shea, “Nonuniform Phase-Shift-Key Modulation for Multimedia Multicast Transmission in Mobile Wireless Networks,” *IEEE J. Select Areas Communication* Volume 17, pp. 774-783, May 1999.
16. M. Pursley and J. Shea, “Multimedia Multicast Wireless Communications with Phase-Shift-Keying and Convolutional Coding,” *IEEE J. Select Areas Communication*, Volume 17, pp. 1999 - 2010, November 1999.

17. A. Annamalai, Jing Lu, and D. R. Vaman, “Improving the Efficiency of Wireless Networks via a Passive Rate-Adaptation Strategy,” *Proc. Wireless Telecommunications Symposium*, pp.370-379, 24-26 April, 2008.
18. Vitthaladevuni, P.K., Alouini, M.-S., "A Recursive Algorithm for the Exact BER Computation of Generalized Hierarchical QAM Constellations," *IEEE Trans Information Theory*, Volume.49, no.1, pp. 297- 307, Jan 2003.
19. P. Vitthaladevuni, M. Alouini, Exact BER Computation of Generalized Hierarchical PSK Constellations,” *IEEE Trans. Communicaiton*, Volume 51, No. 12, , pp. 2030- 2037, Dec. 2003.
20. Olusegun Odejide, Craig Bazil, and Annamalai Annamalai, “Adaptive Multi-resolution Modulation for Multimedia Traffic in Dynamic Wireless Environment,” *IEEE International Conference on Computer Applications & Industrial Electronics (ICCAIE),* December 2010 (Accepted for publication).
21. H.264 and MPEG-4 Video Compression: Video Coding for Next-generation Multimedia by Iain E. G. Richardson, *John Wiley and Sons*, 2007.
22. Abdul H Sadka, Compressed Video Communications, *John Wiley and Sons*, 2002.
23. Video Compression and Communications by L. Hanzo, P. J. Cherriman and J. Streit, *2nd Edition*, John Wiley and Sons, 2007.
24. L.F. Wei, “Coded modulation with unequal error protection,” *IEEE Trans. Commun.*, vol. 41, no. 10, pp. 1439–1449, Oct. 1993.
25. A. R. Calderbank and N. Seshadri, “Multilevel codes for unequal error protection,” *IEEE Trans. Inf. Theory*, vol. 39, no. 7, pp. 1234–1248, Jul. 1993.
26. W. H. Heinzelman and R. Talluri, “Unequal error protection of MPEG-4 compressed video,” *Proc. International Conference of Image Processing*, Vol. 2, pp 530-534, 1999.

27. A. Bhatnagar, S. Kumar, A. Janarthanan, A. Annamalai Jr, M. Medley and J. Matyjas, "A Multilevel Unequal Protection Scheme for Robust H.264/AVC Video Transmission over Wireless Channels," *IEEE MILCOM*, Boston, MA, USA, Oct. 2009.
28. J.Liu and A. Annamalai, "Multiresolution Signalling for Multimedia Multicasting", *Proc IEEE Vehicular Technology Conference*, Fall 2004, pp 1088-1092.
29. Y. C. Chang, S. W. Lee and R. Komiya, "A low complexity unequal error protection of H.264/AVC video using adaptive hierarchical QAM," *IEEE Trans. Consumer Electronics*, Vol. 52(4), Nov 2006, pp. 1153-1158.
30. Digital video broadcasting (DVB): Framing structure, channel coding and modulation for terrestrial television, European Standard 300 744 V1.5.1, *European Telecommunications Standard Institute (ETSI)*, Nov. 2004.
31. Songchar Jiang, Lin, H, Tsou S.K," A new unequal error protection scheme for wireless multimedia transmissions", *TENCON 2007 – 2007 IEEE Region 10 Conference*, Oct. 30 2007, pp. 1-4.
32. "Draft ITU-T recommendation and final draft international standard of joint video specification (ITU-T Rec. H.264/ISO/IEC 14 496-10 AVC," in Joint Video Team (JVT) of ISO/IEC MPEG and ITU-T VCEG, JVTG050r1, 2003.
33. T. Wiegand, G. J. Sullivan, G. Bjøntegaard and A. Luthra, "Overview of the H.264/AVC video coding standard," *IEEE Trans. Cir. Syst. Video Technol.*, vol. 13, pp. 560–576, July 2003.
34. S. Kumar, L. Xu, M. K. Mandal and S. Panchanathan, "Error Resiliency Schemes in H.264/AVC Video Coding Standard," *Elsevier J. Visual Communication and Image Representation* (Special issue on Emerging H.264/AVC Video Coding Standard), Vol. 17(2), pp. 425-450, April 2006.
35. B. Sklar, "Digital Communications – fundamentals and applications", *Prentice Hall PTR*, 2001.
36. Lin S., Costello D., "Error Control Coding: Fundamentals and Applications" *Prentice-Hall*,

Englewood Cliffs, N.J., 1983.

37. A. Viterbi, "Convolutional Codes and Their Performance in Communication Systems," *IEEE Trans. Communication Technology*, Volume 19, Issue 5, Part 1, pp. 751-772, Oct. 1971.
38. J. Hagenauer, "Rate-compatible punctured convolutional codes (RCPC codes) and their applications," *IEEE Trans. Communications*, Volume 36, Issue 4, pp. 389-400, Apr. 1988.
39. L. H. C. Lee, "New rate-compatible punctured convolutional codes for Viterbi decoding," *IEEE Trans. Communications*, Volume 42, Issue 12, pp. 3073-3079, Dec. 1994.
40. Youngkou Lee, Sungsoo Choi, and Kiseon Kim, "Performance of RCPC codes with soft-decision decoding over Nakagami –m fading channels", *IEEE Communs. Letts.*, vol. 6, pp. 31-33, Jan. 2002.
41. A. Roongta, and J. M. Shea, "Reliability based hybrid ARQ and rate-compatible punctured convolutional (RCPC) codes", *Proc. IEEE Wireless Communs. And Networking Conf.*, vol. 4, pp. 2105-2109, 21-25 March 2004.
42. K. Hasung, and G. L. Stuber, "Rate-compatible punctured SCCC codes," *Proc. Vehicular Techol. Conf.*, vol. 4, pp. 2399-2403, Oct. 2001.

LIST OF ACRONYMS

AN	Airborne network
AWGN	Additive white Gaussian noise
BER	Bit error rate
BFGS	Broyden–Fletcher–Goldfarb–Shanno
CNR	Carrier to noise ratio
CSI	Channel side information
ERFC	Complementary error function
GOP	Group of pictures
LAN	Local area network
LSB	Least significant bit
MANET	Mobile ad-hoc network
MSB	Most significant bit
NAL	Network abstraction layer
PAM	Pulse amplitude modulation
PSK	Phase shift keying
PSNR	Peak signal to noise ratio
QAM	Quadrature amplitude modulation
QoS	Quality of service
RCPC	Rate-compatible and punctured convolutional codes
SNR	Signal to noise ratio
TCM	Trellis coded modulation
UEP	Unequal error protection

VCL	Video coding layer